ERDE TR-87

UNLIMITED

ERDE TR 87

BR29465

MINISTRY OF DEFENCE

EXPLOSIVES RESEARCH AND DEVELOPMENT ESTABLISHMENT

TECHNICAL REPORT No. 87

Parallel Plate Plastometry of Plastic Propellant: Part 2: Determination of Plastoviscosity and the Flow Curve Equation

Virginia M Gledhill
W A Dukes

PROPERTY OF U.S. ARMY
STINFO BRANCH
BRL, APG, MD. 21005

DISTRIBUTION STATEMENT A
Approved for Public Release
Distribution Unlimited

COUNTED IN

ERDE TR-87

PD 14318

WALTHAM ABBEY
ESSEX

January
1972

20071011139

MINISTRY OF DEFENCE

EXPLOSIVES RESEARCH AND DEVELOPMENT ESTABLISHMENT

Technical Report No 87

January 1972

Parallel Plate Plastometry of Plastic Propellant: Part 2: Determination of Plastoviscosity and the Flow Curve Equation

by

Virginia M Gledhill
W A Dukes

SUMMARY

The use of the parallel-plate plastometer has been extended to measure the plastoviscosity of a representative plastic propellant over a wide strain-rate range (about 10^{-5} to 10 s^{-1}). The experimental technique is to compress a cylindrical specimen but the results can be analysed in two ways, yielding either zero-strain or finite-strain plastoviscosities respectively. Both plastoviscosities are, within experimental scatter, inversely proportional to the square root of the strain-rate, and range from about 100 to 0.1 MN s/m^2 (1 GP to 1 MP).

The plastoviscosity decreases rapidly and exponentially with increasing strain. When the finite-strain measurements are extrapolated to zero strain, there is good agreement with the zero-strain measurements.

The flow curve for a given strain, relating strain-rate with stress, is parabolic. The yield stress and shear-hardening coefficient (measured separately) have been taken into account, resulting in a complete flow equation linking stress, strain and strain-rate, corresponding to a family of flow curves.

PROPERTY OF U.S. ARMY
STINFO BRANCH
BRL, APG, MD., 21005

Further copies of this technical report can be obtained from Defence Research Information Centre, Station Square House, St Mary Cray, Orpington, Kent. BR5 3RE

CONTENTS

Reference: WAC/213/029

1 INTRODUCTION

Plastic propellant is a stiff paste typically containing (by weight) 89 per cent solids (ammonium perchlorate and perhaps aluminium and a burning catalyst), 1 per cent synthetic surface-active agent and 10 per cent polyisobutene. The polyisobutene has a nominal viscosity-average molecular weight of about 4×10^4 and a viscosity of about 100 kN s/m^2 (10^6 poise) at 25°C, when measured at a very low shear-rate by the falling sphere (Stokes) method. The paste is similar to modelling clay or Plasticine, and may be considered to a first approximation as a Bingham solid subject to shear-hardening.[1]

As part of a programme aimed at characterising rheologically both plastic propellant and its ingredients, detailed consideration has been given to the methods by which the fundamental rheological properties such as viscosity, plastoviscosity, yield stress and shear-hardening coefficient may be measured. A separate report will deal with the liquid ingredients; this report is confined to a consideration of the rheology of plastic propellant itself.

Routine measurements on the very viscous liquid ingredients (usually polyisobutene or mixtures of polyisobutene with plasticisers and surfactants) are made with a falling-sphere viscometer, normally using a steel ball of diameter 2.38 mm falling through a sample in a tube 25 mm wide for periods as long perhaps as 24 hours, before a distance is passed which may be measured with sufficient accuracy. When the liquid is opaque, X-rays are used to measure the distance through which the sphere has fallen. The viscosity is calculated from Stokes' law, after applying the Faxén correction for the wall-effect.

A useful survey[2] of viscometric techniques for use with polymeric liquids summarises the range of viscosities over which various methods are useful and suggests that other methods, such as capillary extrusion, tensile creep and parallel-plate plastometry, might be more suitable for fluids of very high viscosity. Tensile creep experiments have been carried out on plastic propellant, but not yet on its liquid ingredients, and this work will be reported separately. Work on capillary extrusion is planned, both on plastic propellant and on the liquid ingredients.

Other desiderata for a suitable method are listed,[2] including ease of thermostatting, availability of a wide range of shear stresses and shear rates, and applicability to small samples. These considerations support the choice of parallel-plate plastometry in the present work. The size of sample required is small (the whole apparatus may easily be inserted in a laboratory oven or cold chamber) and about a one-hundred-fold range of load is easily available, giving, as will be shown later, about a 10^4 range of shear rates.

The availability of a wide range of shear-rates is important when dealing with polymers, which are usually non-Newtonian, ie their viscosity is not independent of the shear-rate. It has been shown[3] that the mechanical

properties of plastic propellant are highly dependent on the strain-rate, so it is important to consider the effect of this parameter on the rheological properties.

The compression between parallel plates of a sample, often cylindrical, by a constant load has been widely used as an empirical method of measuring the consistency of plastic materials. The main reason for the use of this test is probably that this form of specimen is easily made and handled, even when the material is soft and sticky. Unfortunately the test is not so easily analysed in rheological terms; for example, both stress and strain vary both with position within the specimen and with time. In the previous report in this series[1] the latter variable was not considered, and attention was limited to the equilibrium state when compression is complete. It was shown[1] that the fundamental properties of yield stress and strain-hardening coefficient may be derived from measurement of the equilibrium plate separation. In the present report time-effects are considered, involving such concepts as flow, strain-rate and plastoviscosity.

A routine test for plastic propellant[4] is to apply an axial load (normally 1500 g) to a cylinder (20 mm high and 15 mm diameter) between parallel plates wider than the cylinder, and to record the decrease in height as a function of time. The percentage decrease in height after an arbitrarily chosen time (30 seconds) is termed the 'plasticity value' and the percentage decrease in height at which the surface of the specimen begins to rupture after further compression is termed the 'crack value'. The same test has been used to give an estimate of a more fundamental flow parameter, the 'plastoviscosity' (defined in Section 2 1) but the analysis of the experimental data used to derive this parameter was very empirical. It was assumed[4] as in textbooks on the strength of materials that the mean compressive stress Wg/A (where W is the applied load and A is the cross-sectional area of the specimen) would produce a maximum shearing stress equal to $Wg/3A$ in all planes inclined at 45° to the axis, and that the compressive strain γ_h was given by

$$\gamma_h = -\int_{h_o}^{h} dh/h = \ln (h_o/h) \qquad (1)$$

A plot of $\ln (h_o/h)$ against time was made and extrapolated back to zero time; the initial slope of this curve then gave the initial (ie, at zero strain) rate of strain $\dot{\gamma}_{h,o}$, and this was divided into $Wg/3A$ to give an "apparent plastoviscosity". Strictly speaking, a value for the initial yield stress should be subtracted from the shearing stress, but this is usually a negligible correction since the compressive loads are very much greater than the yield stress. Since this "apparent plastoviscosity" had been found to be invariably 30 to 50 per cent lower than the plastoviscosity determined with a concentric cylinder plastometer, it was multiplied by an empirical conversion factor of 1.5. Thus the routine "apparent initial plastoviscosity" is given by[4]

$$\eta_a = Wg/2A_o \dot{\gamma}_{h,o} \qquad (2)$$

The concentric cylinder plastometer mentioned above has been described elsewhere.[5,6] A few results were reported[6] on plastic propellant containing a mixture of synthetic surface-active agents, similar to current propellants. Both the yield stress and the plastoviscosity were found to be affected by the strain the material had undergone; the yield stress increased linearly with increasing strain, ie the material shear-hardened linearly (as later confirmed by parallel-plate plastometry[1]), and the plastoviscosity decreased with increasing strain.

2 THEORETICAL

2 1 General

The yield stress f_m of a plastic material is the stress below which no flow takes place, ie the strain-rate $\dot{y} = 0$ if the applied stress $\bar{s} \leq f_m$; while in general for $\bar{s} > f_m$ the rheological behaviour is specified by the flow curve

$$\dot{y} = f(\bar{s} - f_m) \tag{3}$$

A Newtonian liquid is specified by the flow curve

$$\dot{y} = \bar{s}/\eta \tag{4}$$

where η is the coefficient of viscosity. Thus for a Newtonian liquid a plot of $\dot{y}$ versus $\bar{s}$ is a straight line through the origin, with slope $1/\eta$. The comparable flow curve for a plastic material obeying Eqn 3 has a finite intercept f_m on the stress axis, and is not necessarily a straight line. (A straight line with finite intercept defines a Bingham material.) The plastoviscosity η_{pl} is defined as the differential $d(\bar{s} - f_m)/d\dot{y}$, that is the inverse of the slope of the $\dot{y}$ versus $(\bar{s} - f_m)$ curve at any value of $\dot{y}$, and is not necessarily invariant with $\dot{y}$. Plastoviscosity is thus the analogue of Newtonian viscosity appropriate to a plastic material.

Non-linear flow curves are exhibited not only by some plastic materials, but also by liquid polymers which have a high viscosity. In this case departure from Newtonian behaviour may be explained as due to chain entanglements. The reduction of the viscosity of such materials with increasing shear rate is termed pseudo-plasticity. Recent papers[7,8] have dealt with this property, and a number of empirical equations has been put forward and discussed.[8] For example, the following equation represents the behaviour of many systems:[8]

$$\eta = \eta_\infty + (\eta_o - \eta_\infty) \Big/ \left[1 + (\tau\dot{y})^n\right] \tag{5}$$

where η is the viscosity at shear rate $\dot{y}$, and η_o and η_∞ are limiting values at $\dot{y} = 0$ and $\dot{y} = \infty$, respectively. τ is a constant such that at a shear rate τ^{-1} the viscosity assumes the mean value $(\eta_o + \eta_\infty)/2$.

If η_∞ is zero, or negligible, and at rates of shear such that $(\tau\dot{y})^n >> 1$, then this becomes

$$\eta = \eta_o/(\tau\dot{y})^n \qquad (6)$$

and a plot of log η against log $\dot{y}$ is linear, with a slope of -n. This is sometimes called the power-law flow equation, and it is applicable to many polymeric liquids and plastic materials. A similar result is obtained[9] for many disperse systems on the basis of a kinetic interpretation, when the contribution of Brownian movement to the rupture of links between particles is negligible compared with that due to applied shear. Eqn 6 may be rewritten

$$\eta = \frac{d\bar{s}}{d\dot{y}} = k\dot{y}^{-n} \qquad (7)$$

By integration, (except when n = 1)

$$\bar{s} - f_m = k(\dot{y}^{1-n})/1 - n \qquad (8)$$

where f_m is the constant of integration, equal to the yield stress (if any). Therefore

$$\dot{y} = \left[\frac{1 - n}{k}(\bar{s} - f_m)\right]^{1/1 - n} \qquad (9)$$

This is the form of the flow curve, generalised in Eqn 3, specific for materials obeying the power-law flow equation. It is an example of the Herschel-Bulkley equation.

2 2 Zero-strain Plastoviscosity

In the routine test described in the Introduction, it was assumed that the maximum shearing stress was Wg/3A, although this was then empirically converted to Wg/2A, to gain better agreement with results from a concentric cylinder plastometer. As summarised previously,[1] it has been established[10] that for a tall cylinder, $h_o \geq 2r_o$, as is the standard specimen (h_o = 20 mm, $2r_o$ = 15 mm), consideration of the exact shear zones gives the maximum stress equal to Wg/2A. This gives excellent theoretical confirmation for the empirical conversion.

There remains however the strain-rate to be considered. This was taken as the rate of change of the compressive strain, ln (h_o/h). However it is suggested that the direction of flow is primarily radially outwards. The axial compressive force may be taken as equivalent to a hydrostatic compression, which causes no plastic strain, coupled with a bi-axial tension,

which causes the radial flow outwards. Thus the radial strain $\gamma_r = \int_r^{r_o} dr/r = \ln (r/r_o)$, is considered more suitable and will be used here, as it was in the previous report in this series.[1] Since $h_o/h = r^2/r_o^2$,

$$\ln (h_o/h) = \gamma_h = 2\ln (r/r_o) = 2\gamma_r \qquad (10)$$

Similarly

$$\dot{\gamma}_h = 2\dot{\gamma}_r \qquad (11)$$

Thus the initial (zero-strain) plastoviscosity, η_i, as distinct from the apparent value η_a defined in Eqn 2, is given by

$$\eta_i = \frac{Wg}{2A_o\dot{\gamma}_{r,o}} = \frac{Wg}{2A_o} \cdot \frac{2}{\dot{\gamma}_{h,o}} = 2\eta_a = \frac{Wg}{A_o\dot{\gamma}_{h,o}} \qquad (12)$$

For the standard specimen this becomes

$$\eta_i = 0.0278\ W(\text{kg})/\dot{\gamma}_{r,o}(\text{s}^{-1}) \quad \text{MN s/m}^2 \qquad (13)$$

The question of the absolute value of the strain and hence of the strain-rate will be considered further in Sections 4 1 3 and 4 2 3, in the light of experimental results.

2 3 Finite-Strain Plastoviscosity

The theory and application of the parallel-plate plastometer have been discussed previously[11,12,13] and for the present purpose it may merely be stated that if a cylindrical sample of volume V is compressed by a constant load W between parallel plates, then a plot of $1/h^4$, where h is the plate separation at time t, against t will give a curve which after the elastic and delayed elastic deformations have taken place becomes linear. From the slope of the linear portion of the curve the plastoviscosity (or viscosity) η_d may be determined, from a modified form of Stefan's equation:

$$\frac{3V^2}{8\pi}\left(\frac{1}{h^4} - \frac{1}{h_o^4}\right) = \frac{Wgt}{\eta_d} \qquad (14)$$

The assumptions on which this analysis is based are as follows:

a the material is incompressible;

b the flow behaviour of the material is Newtonian at the rates of shear employed during a test;

c no body force acts on the material;

d the motion is slow;

e there is no slip at the surface of the plates; and

f the plate separation is so small compared to the radius that the velocity component in the perpendicular direction is negligible compared with that in the radial direction.

These assumptions are commented on below.

Assumption a is satisfied to a first-degree approximation by a void-free liquid or a dispersion of solid particles in a liquid. Assumption b is approximately correct within experimental error, as a linear plot of $1/h^4$ vs t is found while the strain-rate is varying over the relatively small range occurring during a single experiment (ie the change in strain-rate during the period of purely viscous flow is small). Assumption c is reasonable, as the body forces are of the order of millibars, while forces of the order of bars are being applied. Assumption d enables terms in the square of the velocity vector to be neglected in the Navier-Stokes equation. Assumption e has been shown[1] to be correct for plastic propellant. Assumption f was said[11] to be met if the ratio of radius to height of the compressed specimen was greater than 10: we find no inconsistencies with the ratio ranging from as small as 2 or 3 up to 19.

3 EXPERIMENTAL

3 1 Apparatus

The apparatus used was mechanically simple, being essentially a wide circular horizontal brass base-plate, on a threaded coaxial support, enabling it to be raised or lowered by rotation about its axis. The whole apparatus stood on a levelling platform fitted with three adjustable screw legs. Above the base-plate there was another horizontal circular brass plate, 51 mm in diameter, fixed squarely to and supported by a vertical rod (9.5 mm diameter) passing through a low-friction bearing and provided with a concentric circular weight-pan, on which circular slotted weights could be placed. At the top of the rod was rigidly fixed an inverted stirrup fitting through the jaws of a bomb-release mechanism, which supported the rod and upper plate until the mechanism was activated and the jaws sprang apart, when the upper plate with the rod and weights was free to fall. A cylindrical sample of the material to be tested was placed centrally on the lower plate, which was then raised until the top of the sample just touched the upper plate. The experiment was then started by activating the bomb-release mechanism.

Resting on the upper surface of the upper (moving) plate, and supported vertically with little friction was a brass rod (2 mm diameter) supporting a rod-shaped soft-iron core positioned inside the vertical coil assembly of a Schaevitz linear variable differential transformer (Electro Mechanisms Ltd, Slough), which produces an electrical output proportional to the displacement of the core. The output was led to a Sanborn (Hewlett-Packard) model 321 amplifier recorder which when calibrated recorded the plate separation as a function of time. The speed of response of the recorder was more than adequate for the fastest experiments described in this report. The duration of experiments varied between 0.25 second and 1 hour. The available chart speeds were 0.5, 1, 5, 20 and 100 mm/s from which a suitable speed was chosen for each experiment. The loads used ranged from 0.4 to 100 kg. With loads greater than 5 kg, a 10:1 level apparatus was used, with similar instrumentation.

Experience with this apparatus has led to the design of a more convenient and precise instrument, in which calibration is simpler, and which is provided with temperature control. It is hoped that this will facilitate future routine measurements. In the work described in this report, the temperature was not controlled; all experiments were performed at room temperature.

3 2 Material

The plastic propellant used throughout the work described in this report was E3342/Lot 9. Its tensile properties were reported in Reference 3c. Its composition is given in the Appendix. Routine determinations[14] of the plasticity and crack values gave 23% and about 85% respectively. Each cylindrical specimen was made in the standard way, from a single boring of the required weight, with freshly cut surfaces, confined in a lightly-greased mould of the required dimensions between two discs of polytetrafluorethylene (PTFE) film of the required radius at a pressure of 6.9 MN/m^2 for 1 minute. Specimens were pushed out of the mould, and the PTFE discs carefully removed. The volume of specimens ranged from 0.5×10^{-6} to 8.2×10^{-6} m^3, the initial radius r_o was within the range 5 to 10 mm, and the initial height h_o was within the range 3.75 to 30 mm, with the initial aspect ratio h_o/r_o ranging from 0.375 to 6.0.

3 3 Procedure

Each specimen, prepared as described above, was compressed by a known load W, and the plate separation h recorded as a function of time. A typical curve is shown in Fig 1. Plots of $1/h^4$ and of γ_r were then derived, typified by those shown in Fig 2, derived from Fig 1. The initial slope of the γ_r plot is drawn, equal to $\dot{\gamma}_{r,o}$, and this is substituted in Eqn 12 or 13 to derive the zero-strain plastoviscosity, η_i.

The slope $\bar{m}$ of the linear portion of the $1/h^4$ vs t plot enabled the finite-strain plastoviscosity to be determined by substituting in Eqn 14. For the standard specimen this becomes

$$\eta_d = \frac{6.57 \times 10^{-6}\ W(kg)}{\bar{m}(mm^{-4}, s^{-1})}\ MN\ s/m^2 \qquad (15)$$

The time range of this linear relation was noted, and the strain vs time curve examined over this range, and a mean slope drawn, thus deriving the mean strain-rate, $\bar{\dot{y}}_r$, at which the plastoviscosity had been measured. The procedure is illustrated in Fig 2. It will be seen that there is little change in strain-rate during the measurement, as stated in Section 2 3 above. The mean radial strain $\bar{y}_r$ during the measurement is also recorded.

4 RESULTS

4 1 Zero-strain Plastoviscosity

The parameters which have been varied in turn are: the load applied (and hence the strain-rate), the volume of the specimen, and the aspect ratio (initial height/initial radius, h_o/r_o) of the specimen. These are discussed in turn below.

4 1 1 Aspect Ratio and Volume Constant

The largest number of experiments (26) with constant particular values of both the aspect ratio h_o/r_o and the volume V was with the standard specimen (h_o/r_o = 20 mm/7.5 mm = 2.67, V = 3.53×10^{-6} m^3). The heavier the load, the higher was the initial strain rate $\dot{y}_{r,o}$ and the lower the initial viscosity η_i. In Fig 3, log η_i is plotted as a function of log $\dot{y}_{r,o}$. The least-squares regression of log η_i on to log $\dot{y}_{r,o}$ is shown; it has slope -0.54 (= -n, see Eqn 6), with a standard error of estimate 0.14. The material thus obeys the power-law equation.

4 1 2 Aspect Ratio Constant, and Volume Varied

Specimens were made of four different volumes (0.50, 1.8, 4.2 and 8.2×10^{-6} m^3) but with the aspect ratio maintained constant, h_o/r_o = 1.33. These were compressed by various loads. As before, the heavier the load, the higher was the initial strain-rate $\dot{y}_{r,o}$ and the lower the initial viscosity η_i. In Fig 4 it is shown that the volume of the specimen does not affect the relation between initial plastoviscosity and strain-rate. The least-squares regression of log η_i on to log $\dot{y}_{r,o}$ is shown; it has a slope -n = -0.52, with a standard error of estimate 0.09.

4 1 3 Aspect Ratio Varied

Specimens were made of various volumes, with five different aspect ratios (0.375, 0.75, 2.0, 4.0 and 6.0) in addition to the two sets shown in Figs 3 and 4 (with ratios of 2.67 and 1.33 respectively). These were compressed by various loads, and as before the heavier the load, the higher was the initial strain-rate $\dot{y}_{r,o}$ and the lower the initial viscosity η_i. Least-square regressions were not made, but it was clear that for each aspect ratio plots of log η_i against log $\dot{y}_{r,o}$ (analogous to Figs 3 and 4) gave lines of similar slope, but slightly displaced horizontally one from another. For example, the regression line of Fig 3 (h_o/r_o = 2.67) at the centre of the range of log η_i has to be shifted positively (ie, to the right) by 0.2 of a decade in order to coincide with the similar line of Fig 4 (h_o/r_o = 1.33).

The shifts, log $p_{h/r}$, necessary for all the results to be superimposed on a master curve, have been estimated for each aspect ratio, and the shift plotted (as circles) as a function of the natural logarithm of the aspect ratio in Fig 5. The reference aspect-ratio has been taken arbitrarily (for reasons to be discussed below) at 1.55, ie log $p_{1.55} = 0$. From the full line drawn (by eye) in Fig 5, it appears that the shifts are roughly proportional to the logarithm of the aspect ratio:

$$\log p_{h/r} = 0.29 \ln h_o/r_o - 0.14 \qquad (16)$$

$$\text{or } \log p_{h/r} = 0.67 \log h_o/r_o - 0.14 \qquad (16a)$$

It is postulated that the physical significance of these shifts is as follows. (This argument will be reinforced in Section 4 2 3 below.)

It is probable that y_r as defined in Eqn 10 is not an accurate measure of strain, particularly in the case of initially very short cylinders, $h_o/r_o \ll 1$, because there is always[10] a region in contact with each plate near the centre where the material is undisturbed. As h_o/r_o becomes smaller the proportion of the total volume which remains undisturbed will increase, so that the remainder of the material will undergo a greater amount of strain than the apparent radial strain. Evidence supporting this hypothesis has been given,[1] on the basis of the equilibrium separation of cylinders of various aspect ratios, using a strain-hardening material. It is therefore postulated that the shifts log $p_{h/r}$ are associated with this distinction between the radial strain given by y_r ($= \frac{1}{2} \ln h_o/h$) and the actual strain. Thus the shifts are factors which convert the radial strain-rate $\dot{y}_r$ (proportional to y_r) into corrected strain-rate. The higher the aspect ratio, the greater the shift.

The reference aspect-ratio of $h_o/r_o = 1.55$ has been chosen arbitrarily as being near the centre of the experimental range, and also the point at which the tall cylinder ($h \geq 2r$) theory[10] is equated to the short cylinder theory.[1] It was assessed[1] that for standard specimens compressed to equilibrium the quoted radial strain y_r was not more than 10 per cent less than the probable true strain; but the divergence will be greater for cylinders at nearly zero strain, as when deriving η_i.

The strain-rate $\dot{y}_r$ to be corrected in this way appears not only as the abscissa of plots (like Figs 3 and 4) of log η_i against log $\dot{y}_{r,o}$, but also inversely in the derivation of η_i (see Eqn 12). Thus a positive horizontal shift log $p_{h/r}$ as found empirically above should, in order to conform to this hypothesis, be considered as the combination of a positive horizontal shift with an equal negative vertical shift; that is to say a resolved shift of $\sqrt{2}$ log $p_{h/r}$ along a locus with slope -1. The master-curve of all the 74 determinations of η_i has been derived in this way, using smoothed values of log $p_{h/r}$ from the line in Fig 5, and is shown in Fig 6. It may be noted that the shifts are small when compared to the experimental ranges of both log η_i and log $\dot{y}_{r,o}$.

The equation of the regression line, as drawn, is

$$\log \eta_i/p_{h/r} = -0.275 - 0.514 \log \dot{\gamma}_{r,o} \cdot p_{h/r} \qquad (17)$$

The correlation coefficient is -0.97 and the standard error of estimate of the logarithm of the initial plastoviscosity is 0.13. Thus, within experimental error, the initial plastoviscosity is inversely proportional to the square-root of the strain-rate:

$$\eta_i/p_{h/r} = 0.53(\dot{\gamma}_{r,o} \cdot p_{h/r})^{-\frac{1}{2}} \quad \text{MN s/m}^2 \qquad (17a)$$

This equation may be compared with the general form of Eqn 7.

4 2 Finite-strain Plastoviscosity

The parameters varied in the finite-strain plastoviscosity determinations were the same as for the zero-strain determinations described in Section 4.1; namely the applied load (and hence the strain-rate), the specimen volume and the initial aspect ratio. Indeed the same specimens were used; the compression of each was continued, so that Eqn 15 could be applied in the way described in Section 3 3. The parameters are discussed in turn below.

4 2 1 Aspect Ratio and Volume Constant

The same specimens as described in Section 4 1 1 were used. The heavier the load, the higher was the mean strain-rate $\bar{\dot{\gamma}}_r$ and the lower the plastoviscosity η_d. In Fig 7 $\log \eta_d$ is plotted as a function of $\log \bar{\dot{\gamma}}_r$. The least-squares regression of $\log \eta_d$ on to $\log \bar{\dot{\gamma}}_r$ is shown; it has a slope $-n = -0.52$, very similar to the previous results with the zero-strain plastoviscosity η_i, but with a standard error of estimate 0.38, as compared with 0.14 for $\log \eta_i$ in Fig 3. The much greater scatter is presumably due to an additional factor, not operative in the case of the zero-strain experiments. The most obvious difference between finite-strain and zero-strain determinations is of course the strain, and so the effect of varying the strain was examined in addition to the other parameters (Section 4 2 3 below).

4 2 2 Aspect Ratio Constant, and Volume Varied

The same specimens as described in Section 4 1 2 were used. The heavier the load, the higher was the mean strain-rate $\bar{\dot{\gamma}}_r$ and the lower the plastoviscosity η_d. In Fig 8 it is shown that the volume of the specimen does not affect the relation between plastoviscosity and strain-rate, just as it did not in the case of the initial plastoviscosity (Fig 4). The least-squares regression of $\log \gamma_d$ on to $\log \bar{\dot{\gamma}}_r$ is shown; it has a slope $-n = -0.52$, with a standard error of estimate 0.29, as compared with 0.09 for $\log \eta_i$ in Fig 4. Again the much greater scatter is presumably due to an additional factor, postulated to be the strain, and so the effect of varying the strain will be examined (Section 4 2 3 below).

4 2 3 Strain-Rate Normalised, Aspect Ratio and Strain Varied

The same specimens as described in Section 4 1 3 were used, and measurements were made of the plastoviscosity η_d as usual. In order to investigate the effect of varying both the aspect ratio and strain, it was necessary to remove the variable of the strain-rate. There is good evidence, in Figs 3, 4, 6, 7 and 8, of the effect of the strain-rate on the plastoviscosity. The power-law is obeyed, with exponents 0.54, 0.52, 0.51, 0.52 and 0.52 respectively, all of which are, within experimental variation, negligibly different from 1/2.

Therefore each determination of η_d was normalised to an arbitrary strain-rate ($\log \bar{\dot{\gamma}}_r = \bar{2}$), chosen as being near to the centre of the experimental range. The equation used to convert the logarithm of the measured plastoviscosity, $\log \eta_d$, to the normalised form, $\log \eta_{d\bar{2}}$, is as follows

$$\log \eta_{d\bar{2}} = \log \eta_d + \tfrac{1}{2}(\log \bar{\dot{\gamma}}_r + 2) \qquad (18)$$

The same specimens as described in Section 4 1 1 (the largest group, all with $h_o/r_o = 2.67$) enable the influence of the mean strain $\bar{\gamma}_r$ on the strain-rate-normalised plastoviscosity $\eta_{d\bar{2}}$ to be evaluated. In Fig 9 $\log \eta_{d\bar{2}}$ is plotted as a function of $\bar{\gamma}_r$. The strain strongly influences the normalised plastoviscosity, as postulated in Sections 4 2 1 and 4 2 2 above. The greater the strain, the lower is the plastoviscosity. A linear relation is suggested, and the least-squares regression of $\log \eta_{d\bar{2}}$ on to $\bar{\gamma}_r$ is shown, with correlation coefficient -0.92, slope -1.90, and a standard error of estimate 0.15, which may be compared with that for Fig 7 (0.38), from which the strain-effect had not been isolated.

It was then necessary to find whether this strain-effect on the plastoviscosity is affected by the other parameters, namely the volume and aspect ratio of the specimen.

Based on the specimens described in Section 4 1 2, with various volumes, but all of aspect ratio $h_o/r_o = 1.33$, the effect of the mean strain on the plastoviscosity is shown in Fig 10. It appears that the volume of the specimen does not affect the relation between $\log \eta_{d\bar{2}}$ and $\bar{\gamma}_r$. The least-squares regression is shown, with a slope of -1.68 and a standard error of estimate 0.07, as compared with 0.29 for Fig 8, from which the strain-effect had not been isolated.

The specimens with various aspect ratios, described in Section 4 1 3 were used, together with the results shown in Figs 9 and 10 ($h_o/r_o = 2.67$ and 1.33 respectively) to investigate the effect of the aspect ratio on the relation between strain and strain-rate-normalised plastoviscosity. It was clear that for each aspect ratio plots of $\log \eta_{d\bar{2}}$ against $\bar{\gamma}_r$ (analogous to Figs 9 and 10) gave lines of similar slope, but displaced horizontally one from another. For example, the regression line of Fig 9 ($h_o/r_o = 2.67$) at the centre of the range of $\log \eta_{d\bar{2}}$ has to be shifted negatively (ie to the left) by 0.19 in order to coincide with the similar line of Fig 10 ($h_o/r_o = 1.33$).

It is postulated that the physical significance of these shifts is the same as that of those described above; the difference between the radial strain γ_r and corrected strain becomes greater as the cylinders become squatter. The increase in strain leads to a reduction in plastoviscosity (Figs 9 and 10), so that the shifts are positive for low aspect ratios and negative for high (ie in the opposite sense to the strain-rate shifts, $\log p_{h/r}$).

The shifts, $q_{h/r}$, necessary for all the results to be superimposed on a master curve have been estimated for each aspect ratio, and plotted (as crosses) as a function of the natural logarithm of the aspect ratio, in Fig 5. The reference aspect-ratio has been taken as 1.55, as before. These shifts are very similar to the previous ones, $\log p_{h/r}$, but are more regular. They are linearly related to the logarithm of the aspect ratio: the equation of the pecked line is

$$-q_{h/r} = 0.25 \ln h_o/r_o - 0.11 \qquad (19)$$

$$\text{or } -q_{h/r} = 0.58 \log h_o/r_o - 0.11 \qquad (19a)$$

It is clear from Fig 5 that within experimental accuracy the two shifts, namely $\log p_{h/r}$ in terms of $\log \dot{\gamma}_{r,a}$ and $-q_{h/r}$ in terms of $\bar{\gamma}_r$, are equivalent and are best described by Eqn 19. Thus

$$\log p_{h/r} = -q_{h/r} = 0.25 (\ln h_o/r_o - \ln (h/r)_{ref}) \qquad (20)$$

where $(h/r)_{ref}$ is the reference aspect ratio (= 1.55). That is to say that the aspect ratio affects to the same degree both the strain and the strain-rate, as indeed would be expected.

4 2 4 Strain-Rate and Aspect Ratio Normalised, and Strain Varied

Now that the effects of both the strain-rate and the initial aspect ratio have been isolated, the effect of the strain on the plastoviscosity can be examined. In Fig 11 is shown the strain-rate-normalised plastoviscosity as measured on all 74 specimens (of every initial aspect ratio), as a function of $(\bar{\gamma}_r + q_{h/r})$, the strain normalised to $h_o/r_o = 1.55$. The least-squares regression equation is

$$\log \eta_{d\bar{2}} = 0.932 - 1.88 (\bar{\gamma}_r + q_{h/r}) \qquad (21)$$

and the standard error of estimate of the logarithm of the normalised plastoviscosity is 0.35.

The coefficient of this effect, namely of increasing strain reducing the plastoviscosity, is designated $\underline{b}$, and is equal to 1.88 here. The effect may be termed strain-thinning, as distinct both from the shear-hardening

coefficient, designated[1] a, and from shear-thinning, which is defined[15] as a reduction of viscosity with increasing rate of shear. Thus it is true that plastic propellant exhibits all three properties; namely shear-hardening[1] (that is a strain-dependent increase in yield stress), strain-thinning (ie a strain-dependent reduction in plastoviscosity), and shear-thinning (a strain-rate-dependent reduction in plastoviscosity - see Figs 3, 4, 6, 7 and 8).

4 2 5 Aspect Ratio and Strain Normalised, and Strain Rate Varied

Now that the strain-thinning coefficient b and the minor effect of the initial aspect ratio on the strain and the strain-rate have both been evaluated, it is possible to eliminate the effect of both by extrapolating to zero strain, using the following equation

$$\log \eta_{d,o} = \log \eta_d + b\,(\bar{\gamma}_r + q_{h/r}) \qquad (22)$$

In this way the effect of strain-rate on the finite-strain plastoviscosity η_d can be isolated. Fig 12 shows a plot of all the determinations of η_d thus normalised, as a function of $\log \bar{\dot{\gamma}}_r$. The equation of the regression line, as drawn, is

$$\log \eta_{d,o} = -0.226 - 0.560 \log \bar{\dot{\gamma}}_r \qquad (23)$$

and the correlation coefficient is -0.99 and the standard error of estimate of $\log \eta_{d,o}$ is 0.09. Thus, within experimental error, the finite-strain plastoviscosity is inversely proportional to the square root of the strain-rate:

$$\eta_{d,o} = 0.59(\bar{\dot{\gamma}}_r)^{-\frac{1}{2}} \quad \text{MN s/m}^2 \qquad (23a)$$

This equation may be compared with the general form of Eqn 7.

5 COMPARISON OF EXPERIMENTAL METHODS

Two different sets of experiments have been carried out: the measurement of (a) the zero-strain plastoviscosity, and (b) the finite-strain plastoviscosity. With the effect of the strain now isolated and evaluated, extrapolation of the latter to zero strain (as in Fig 12) enables a direct comparison of the two experimental methods to be made. In each case the minor effect of the initial aspect ratio on the strain and hence the strain-rate has been normalised.

The zero-strain measurements were shown in Fig 6 and described by Eqn 17

$$\log \eta_i/p_{h/r} = -0.275 - 0.514 \log \dot{y}_{r,o} \cdot p_{h/r} \qquad (17)$$

with the correlation coefficient -0.97 and the standard error of estimate 0.13.

The finite-strain measurements extrapolated to zero-strain were shown in Fig 12 and described by Eqn 23

$$\log \eta_{d,o} = -0.226 - 0.560 \log \bar{\dot{y}}_r \qquad (23)$$

with the correlation coefficient -0.99 and the standard error of estimate 0.09.

The two lines are very similar in slope, and cross at log $\dot{y}$ = 1.06. They are shown again in Fig 13, together with the confidence limits (± two standard errors of estimate = 2 × 0.13) of the regression of the bulked data (148 points), shown as pecked lines. The correlation coefficient is -0.99. The equation of the regression line is

$$\log \eta_{pl} = \bar{1}.714 - 0.57 \log \dot{y} \quad ; \quad y = 0 \qquad (24)$$

Thus the bulked zero-strain plastoviscosity is, within the experimental scatter, inversely proportional to the square root of the strain-rate:

$$\eta_{pl} = 0.518(\dot{y})^{-\frac{1}{2}} \quad \text{MN s/m}^2; \quad y = 0 \qquad (24a)$$

Thus the two experimental methods show reasonable agreement.

The agreement would be improved if allowance were made for the probability, discussed in Section 4 1 3, that the true strains are some 10 per cent greater than the quoted radial strains. Allowance for this would shift the line for log $\eta_i/p_{h/r}$ (in Fig 6) both downwards and to the right by 0.1 of a decade, and the line for log $\eta_{d,o}$ (in Fig 12) downwards by a distance 1.88 (= b) times as much. If the divergence between true and quoted strains were as much as 15%, this would result in the two lines crossing near the centre of the strain-rate range, and the agreement between the two experimental methods would be maximised.

6 THE FLOW CURVE EQUATION

A convenient method of summarising the flow properties of a material is by the flow, or consistency, curve, that is a plot of the rate of shear against the shear stress. The flow curves for both Newtonian liquids and Bingham materials were described in Section 2 1: they are straight lines respectively

passing through the origin or with a finite intercept on the stress axis. The experimental measurements of the plastoviscosity of plastic propellant described in Section 4 now enable the form of the consistency curve for this material to be established. That is, the function in Eqn 3 can be defined, as follows.

We have the equation for the bulked experimental results for the strain-rate effect on the zero-strain plastoviscosity:

$$\log \eta_{pl} = \bar{1}.714 - 0.57 \log \dot{y} \quad ; \quad y = 0 \tag{24}$$

Now also taking into account the strain-thinning effect (as in Eqn 21) together with the relation between the initial aspect ratio and the strain (as in Eqn 19), we have

$$\log \eta_{pl} = \bar{1}.714 - 0.57 \log \dot{y} - 1.88 \left\{ \bar{y}_r - 0.25 \ln (h_o/r_o) + 0.11 \right\} \tag{25}$$

Since it has already been shown with parallel plate plastometry the experimental accuracy is such that the power of 0.57 is indistinguishable statistically from 1/2, and since the aspect-ratio correction to the strain is negligible (a few tenths), this may be simplified to

$$\log \eta_{pl} = \bar{1}.714 - 0.5 \log \dot{y} - 1.88y \tag{26}$$

or

$$\eta_{pl} = 0.518 \times 10^{-1.88y} \cdot \dot{y}^{-\frac{1}{2}} \quad \text{MN s/m}^2 \tag{26a}$$

or

$$\eta_{pl} = 0.518 \times 10^{6} \times e^{-4.33y} \cdot \dot{y}^{-\frac{1}{2}} \quad \text{N s/m}^2 \tag{26b}$$

Now the plastoviscosity is defined as $d\bar{s}/d\dot{y}$, and so by integration we have

$$\bar{s} = 1.04 \times 10^{6} \dot{y}^{\frac{1}{2}} e^{-4.33y} + f_m \quad \text{N/m}^2 \tag{27}$$

where f_m is the constant of integration, equal to the yield stress. Thus

$$\dot{y} = 0.93 \times 10^{-12} (\bar{s} - f_m)^2 \cdot e^{8.66y} \quad \text{s}^{-1} \tag{28}$$

It has been shown[1] that plastic propellant shear-hardens linearly, ie the yield stress increases linearly with the strain:

$$f_m = f_o + ay \tag{29}$$

where f_o is the yield stress at zero strain. A batch of the plastic propellant used in this report had values as follows, measured by the methods previously described:[1] $f_o = 5.8$ kN/m^2, $a = 0.6$ kN/m^2. (A second batch showed nearly no shear-hardening, with $f_o = 3.7$ kN/m^2.)

Thus we arrive at the equation for the flow curves at various values of y:

$$\dot{y} = 0.93 \times 10^{-12} \left\{ \bar{s} - (f_o + ay) \right\}^2 \cdot e^{8 \cdot 66y} \quad s^{-1} \qquad (30)$$

This is a form of Eqn 9, which is specific for materials obeying the power-law flow equation.

The flow curves at various values of y are shown (a) in Fig 14, over the full experimental range of strain-rate, (b) in Fig 15, where the area near the origin of Fig 14 is enlarged with the $\dot{y}$ scale 100X and the $\bar{s}$ scale 10X, and (c) again in Fig 16, where the area near the origin of Fig 15 is similarly enlarged. The parts of the curves in Fig 16 within 5 mm of the $\bar{s}$-axis represent extrapolation beyond the lower limit of the experimental strain-rate range, and the effect of shear-hardening is still not distinguishable.

If the curves are further enlarged, that is to say extrapolated to strain-rates of the order of 1 year^{-1} rather than 1 day^{-1}, then the effect of shear-hardening is no longer negligible. Fig 17 represents a three-dimensional model illustrating how if stresses only slightly greater than f_o were to be imposed, the strain-rate would at first increase, and then decrease to zero. Similarly, if a very slow constant strain-rate were imposed, the stress would at first decrease, and later increase. However, this extrapolation may not be justified: as the strain-rate tends to zero the plastoviscosity probably becomes independent of strain-rate.

7 CONCLUSION

A previous report[1] described the use of the parallel-plate plastometer to measure the static quantities of yield stress and shear-hardening coefficient of plastic propellant.

This report records the extension of the use of the same instrument in order to measure the time-dependent flow properties of the same material over a wide range of strain-rates. The effect of the strain-rate on the plastoviscosity has been determined, and it has been established that the strain undergone also strongly affects the plastoviscosity. The equation of the flow curves, ie the relation between stress, strain-rate and strain, has been derived; and to this has been added the yield-stress determinations as previously established,[1] enabling the flow-curves to be constructed over a strain-rate range of nearly a million-fold, from about 10 s^{-1} to about 1 d^{-1}, and a strain range up to about unity.

The flow-curve equation,

$$\dot{\gamma} = 0.93 \times 10^{-12} \left\{ \bar{s} - (f_o + a\gamma) \right\}^2 \cdot e^{8 \cdot 66\gamma} \quad s^{-1} \qquad (30)$$

is, not surprisingly, quite complex, since plastic propellant is a very heavily loaded dispersion of solids in a highly viscous polymer. It should enable the prediction of the deformation behaviour of the material in other forms of laminar flow, and indeed this should be a useful test of its validity. One attempt has already been made in this direction,[16] in which the form of the velocity profile in tubular flow has been derived from Eqn 30 and shown to be a cubic curve at the wall, flattened exponentially towards the centre. Excellent semi-quantitative agreement with experiment was achieved.

With the flow equation established, and the rheological properties of representative plastic propellant formulations thus characterised, it should be possible to estimate the ease with which a rocket motor charge may be formed, and to calculate the resistance of the charge to further deformation, caused, for example, by gravity during storage and by axial acceleration during launching.

8 ACKNOWLEDGEMENTS

Thanks are due to Mr P R Freeman for helpful discussions and for the suggestion to vary the volume and the aspect ratio of specimens in order to achieve a variety of strains, to Mr R W Bryant also for helpful discussions, and to Mr G J Spickernell for samples of propellant.

9 REFERENCES

1	Dukes W A	Parallel Plate Plastometry of Plastic Propellant: Part 1: Determination of Yield Stress. ERDE Report No 14/R/67; Proc 5th Int Congress on Rheology, ed S Onogi, University of Tokyo Press, 1970, Vol 2, p 315
2	Fox T G, Gratch S, Loshaek S	Viscosity Relationship for Polymers, in Rheology, ed F R Eirich, Academic Press, 1960, Vol 1, p 431 ff
3	Bryant R W, Dukes W A, Gledhill R A	Tensile Properties of Plastic Propellants: (a) RD 2404/Lot 19 - ERDE Tech Memo 5/M/69 (b) RD 2428 - ERDE Tech Note 11, 1970 (c) RD 2435, E3342 and E4058 - ERDE Tech Note 13, 1970
4		Joint Services Textbook of Guided Weapons, Pt 6, 1959, para 195
5		ibid, para 187
6	Freeman P R, Thomas A J B, Vernon J H C	Plastic Propellant: The Use of the Ward Plastometer to Study Rheological Properties. ERDE Tech Memo No 12/M/60
7	Bueche F	Viscosity of Entangled Polymers; Theory of Variation with Shear Rate. J Chem Phys, 48(10), 4781 (1968)
8	Cross M M	Polymer Rheology: Influence of Molecular Weight and Polydispersity J Appl Polymer Sci 13, 765 (1969)
9	Idem	Kinetic Interpretation of Non-Newtonian Flow J Colloid Interf Sci, 33(1), 30 (1970)
10	Meyerhof G G, Chaplin T K	The Compression and Bearing Capacity of Cohesive Layers Brit J Appl Phys 4, 20 (1953)
11	Dienes G J, Klemm H F	Theory and Application of the Parallel Plate Plastometer. J Appl Phys, 17, 458 (1946)

12	Dienes G J	Viscoelastic Properties of Thermoplastics at Elevated Temperatures J Colloid Sci, 2, 131 (1947)
13	Oka S	Principles of Rheometry, in Rheology, ed F R Eirich, Academic Press, 1960, Vol 3, p 73 ff
14		Joint Services Textbook of Guided Weapons, Pt 6, 1959, paras 149 ff
15	Reiner M, Scott Blair G W	Rheological Terminology, in Rheology, ed F R Eirich, Academic Press, 1967, Vol 4, p 480
16	Chudyszewicz, Virginia M, Dukes W A	Plastic Propellant Rheology: The Velocity Profile in Tubular Flow ERDE Tech Note 30, 1971

APPENDIX

COMPOSITION OF PLASTIC PROPELLANT E3342
(parts by weight, per cent)

Ammonium perchlorate	77
Ammonium picrate	10
Titanium Dioxide	1
S101 surfactant mixture	1
*B146	11

*B146 = (Polyisobutylene 15
(Ethyl Oleate 2

NOTATION

a	shear-hardening coefficient (Ref 1)
A	cross-sectional area of the specimen
A_o	initial cross-sectional area of the specimen
b	strain-thinning coefficient
f_m	yield stress
f_o	yield stress at zero strain
g	acceleration due to gravity
h	height of the specimen
h_o	initial height of the specimen
h_o/r_o	initial aspect ratio of the specimen
$(h/r)_{ref}$	reference aspect ratio (= 1.55)
k	constant of proportionality
ln	natural logarithm
log	logarithm to the base 10
$\bar{m}$	slope (Eqn 15)
n	power in equations 5 ff
$p_{h/r}$	aspect ratio shift factors (Eqn 16)
$q_{h/r}$	aspect ratio shifts (Eqn 19)
r	radius of the specimen
r_o	initial radius of the specimen
$\bar{s}$	applied stress
t	time
V	volume of the specimen
W	applied load
y	strain

γ_h	compressive strain
γ_r	radial strain
$\bar{\gamma}_r$	mean radial strain
$\dot{\gamma}_h$	rate of compressive strain
$\dot{\gamma}_r$	rate of radial strain
$\bar{\dot{\gamma}}_r$	mean rate of radial strain
$\dot{\gamma}$	strain rate
$\dot{\gamma}_{h,o}$	the initial rate of compressive strain
$\dot{\gamma}_{r,o}$	the initial rate of radial strain
η	viscosity
η_a	apparent initial plastoviscosity
η_d	plastoviscosity defined in Eqn 14
$\eta_{d\bar{2}}$	plastoviscosity normalised to $\log \bar{\dot{\gamma}} = \bar{2}$ (Eqn 18)
$\eta_{d,o}$	plastoviscosity normalised to $\gamma = 0$ and $(h/r)_{ref}$ (Eqn 22)
η_i	initial plastoviscosity
η_o	viscosity at zero shear-rate
η_{pl}	plastoviscosity
η_∞	viscosity at infinite shear-rate
τ	a constant (Eqn 5)

S No 47/72/CJ

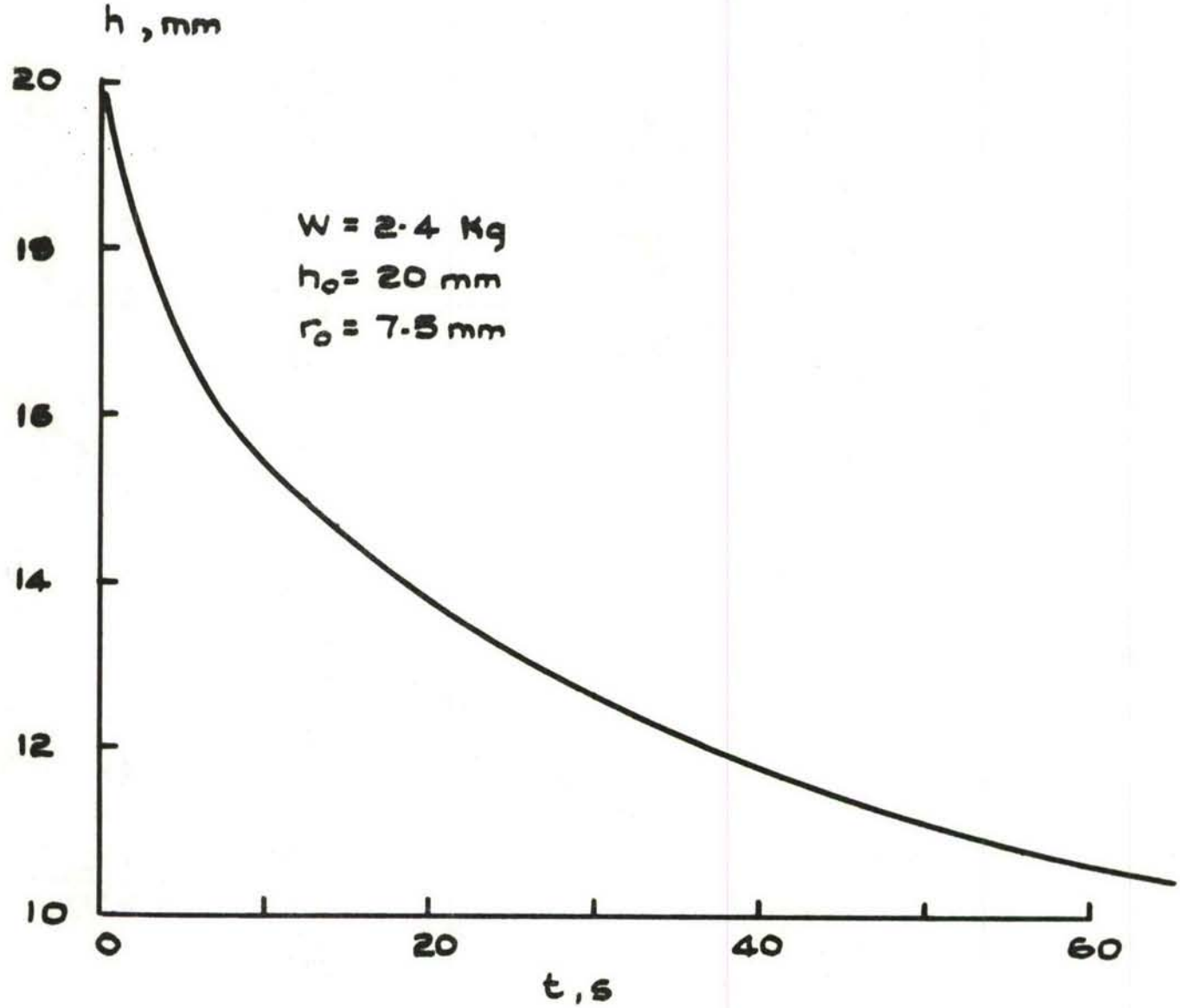

FIG. 1 TYPICAL VARIATION OF SAMPLE HEIGHT DURING COMPRESSION.

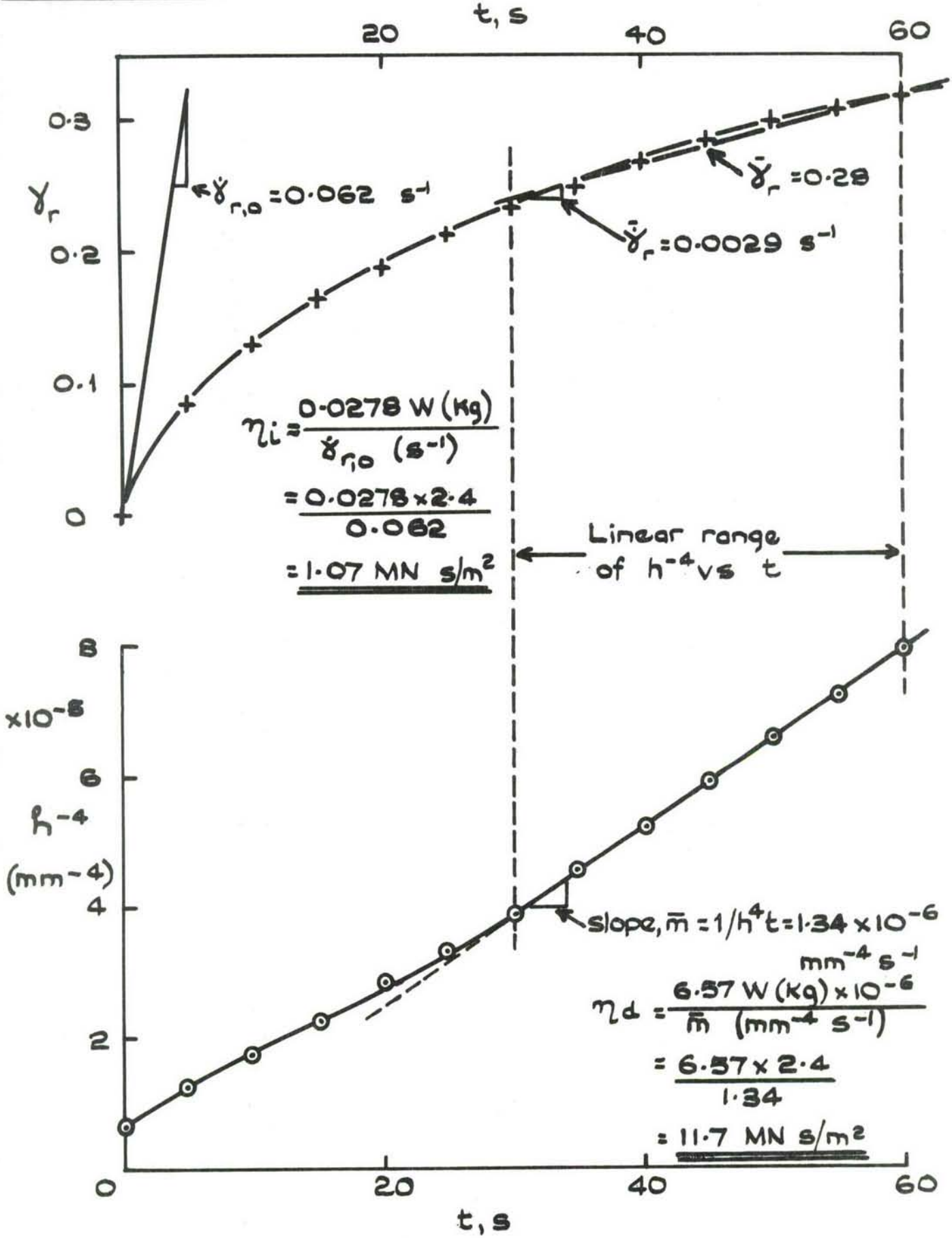

FIG. 2 TYPICAL DETERMINATIONS OF ZERO-AND FINITE-STRAIN PLASTOVISCOSITIES, η_i and η_d

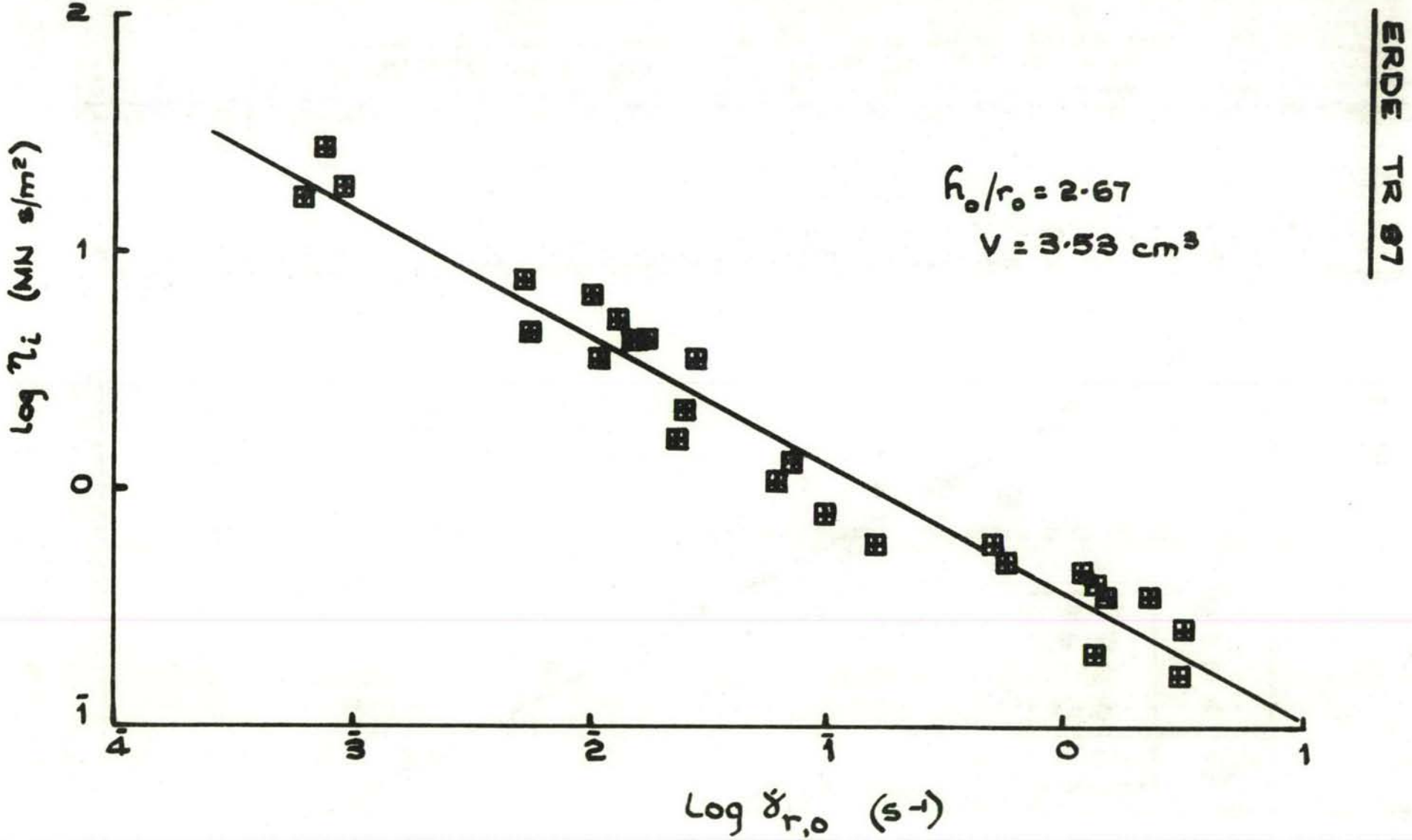

FIG. 3 THE EFFECT OF STRAIN-RATE ON ZERO-STRAIN PLASTOVISCOSITY (INITIAL ASPECT RATIO AND VOLUME CONSTANT)

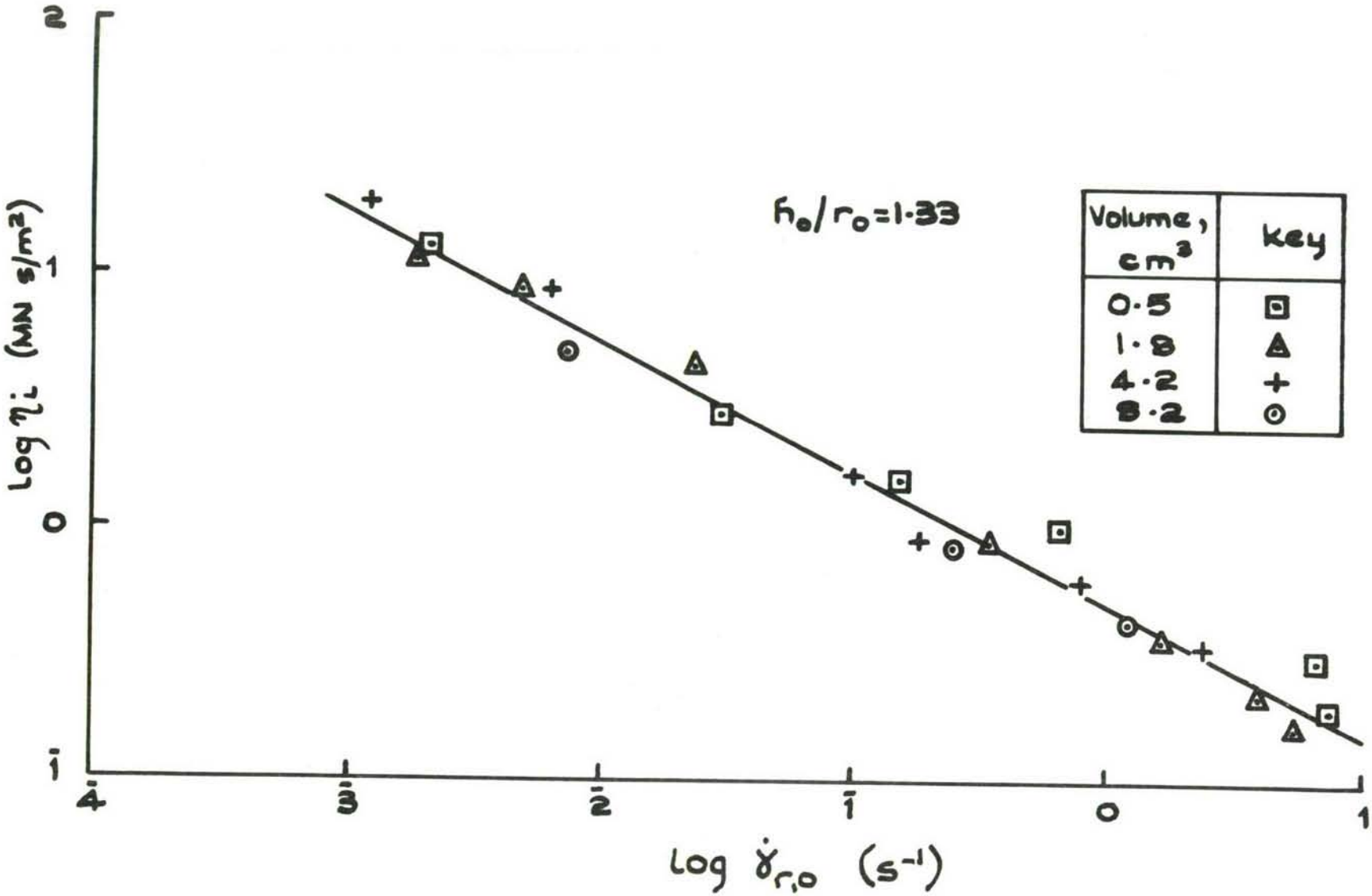

FIG. 4 THE EFFECT OF VOLUME AND STRAIN-RATE ON ZERO-STRAIN PLASTOVISCOSITY (INITIAL ASPECT RATIO CONSTANT)

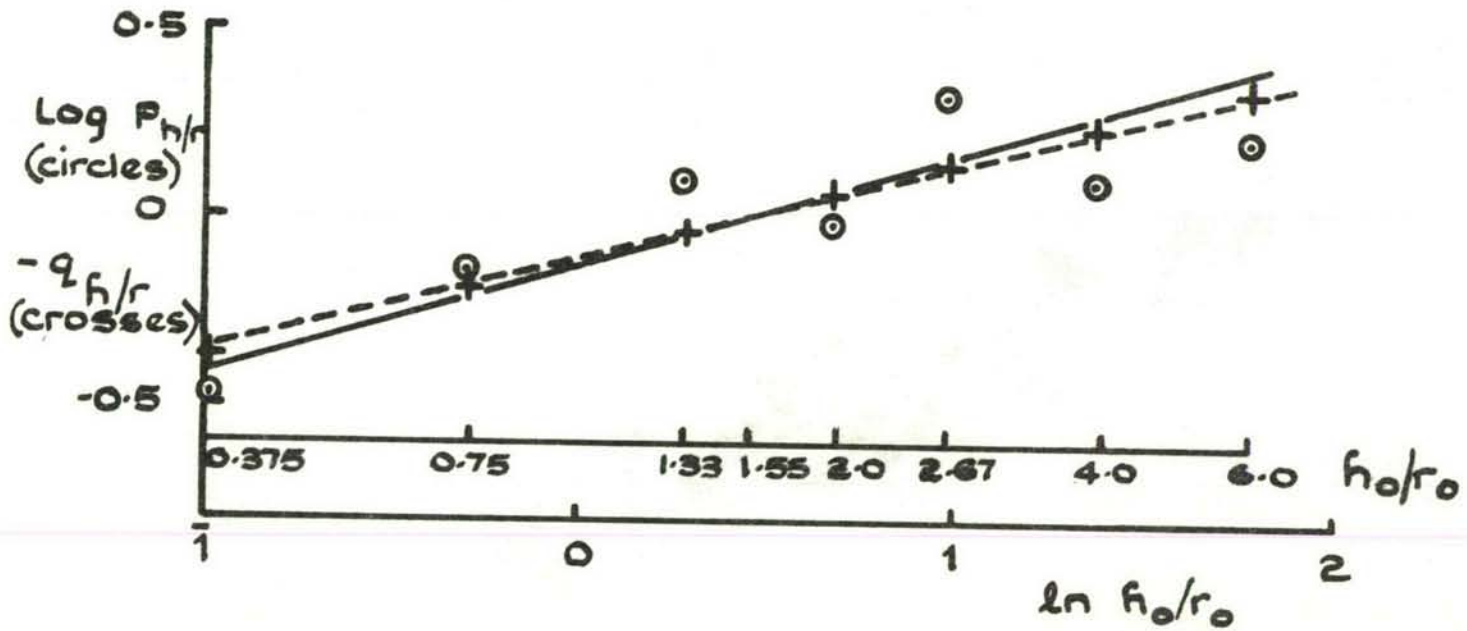

FIG. 5 THE INITIAL-STRAIN-RATE SHIFTS ($\log P_{h/r}$) AND THE STRAIN SHIFTS ($-q_{h/r}$) AS A FUNCTION OF THE INITIAL ASPECT RATIO.

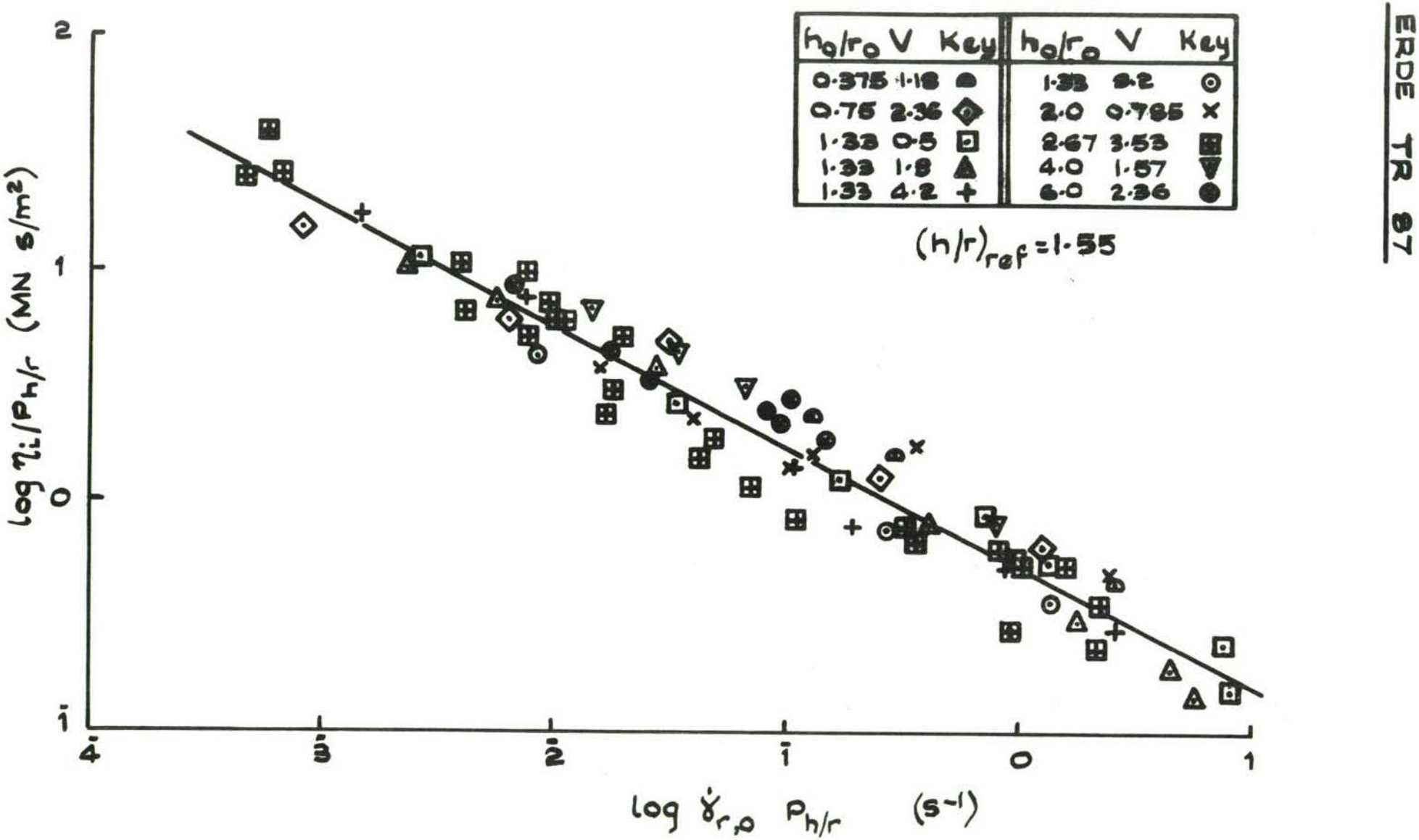

FIG. 6 THE EFFECT OF STRAIN-RATE ON ZERO-STRAIN PLASTOVISCOSITY, BOTH NORMALISED TO AN INITIAL ASPECT RATIO OF 1·55

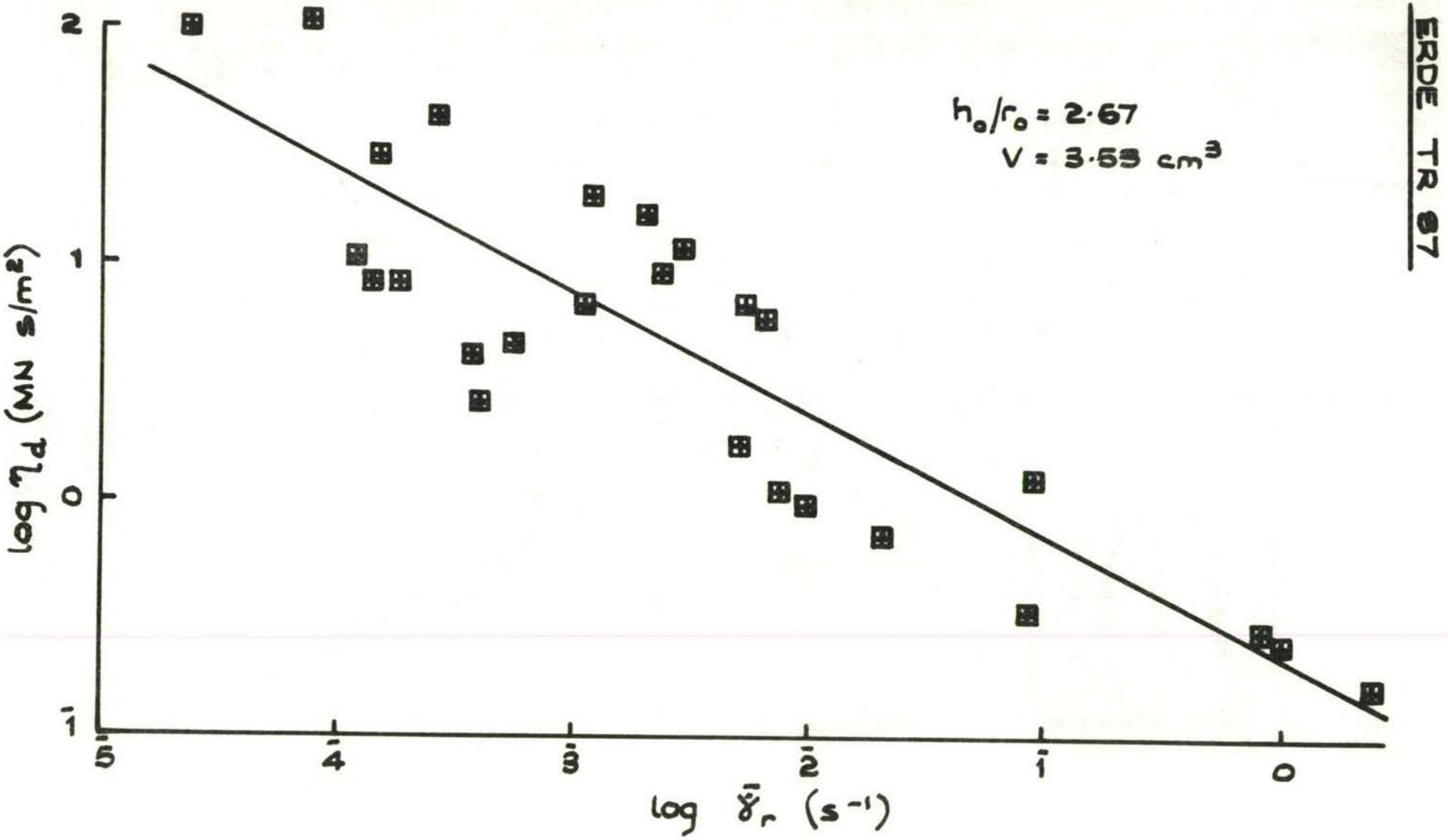

FIG. 7 THE EFFECT OF STRAIN-RATE ON FINITE-STRAIN PLASTOVISCOSITY (INITIAL ASPECT RATIO AND VOLUME CONSTANT)

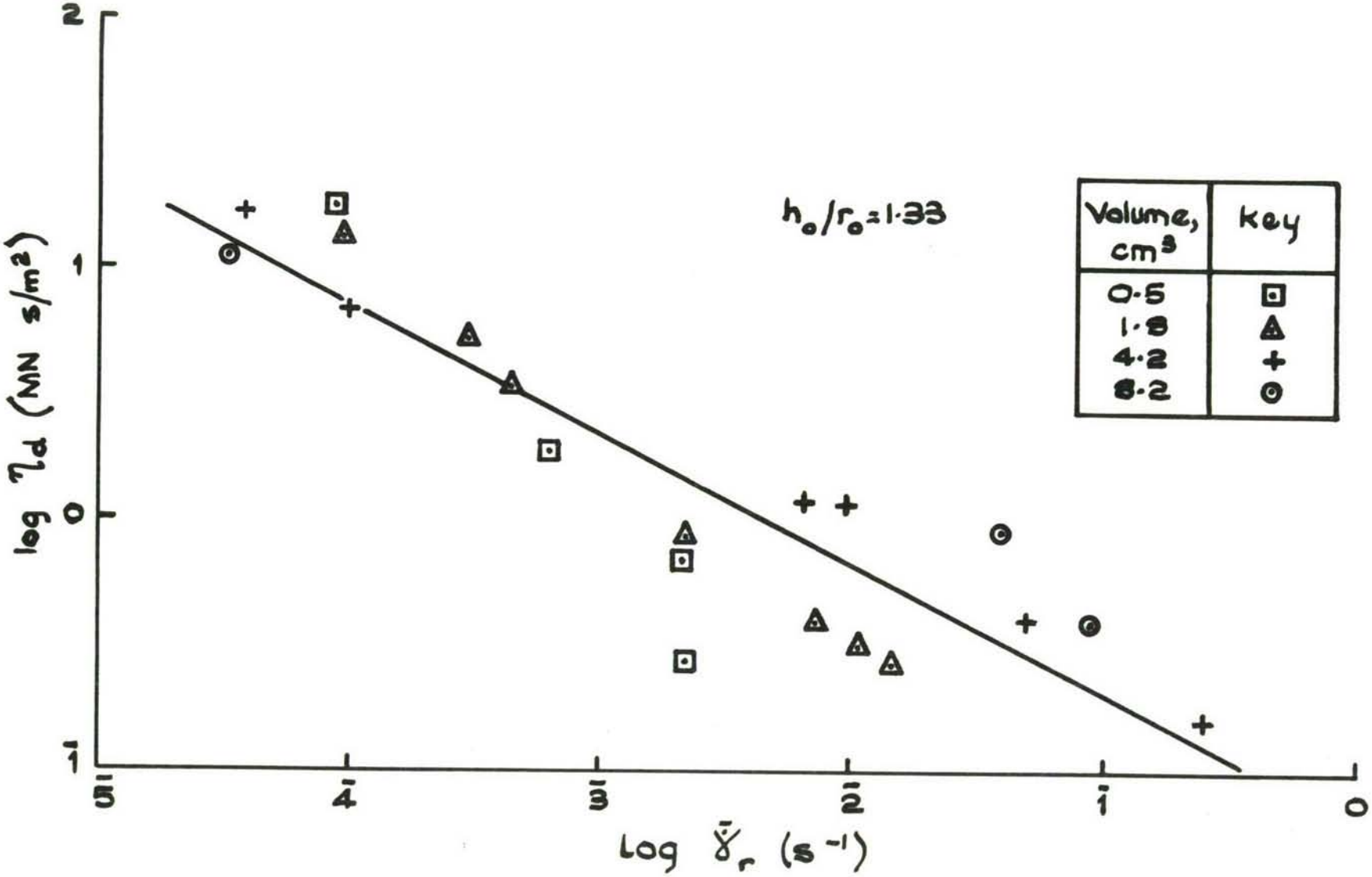

FIG. 8 THE EFFECT OF VOLUME AND STRAIN-RATE ON FINITE-STRAIN PLASTOVISCOSITY (INITIAL ASPECT RATIO CONSTANT)

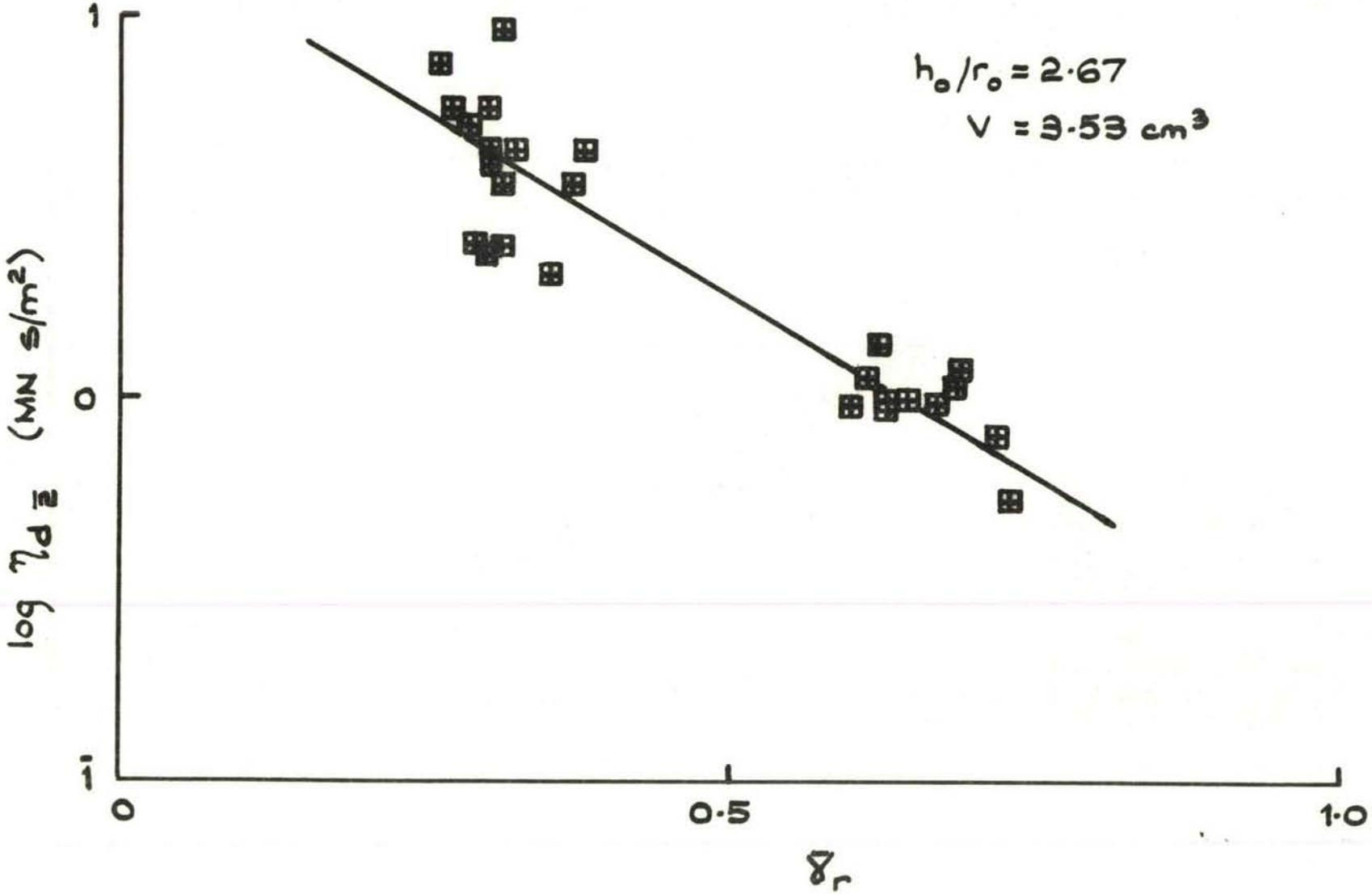

FIG. 9 THE EFFECT OF MEAN STRAIN ON FINITE-STRAIN PLASTOVISCOSITY (STRAIN-RATE NORMALISED; INITIAL ASPECT RATIO AND VOLUME CONSTANT)

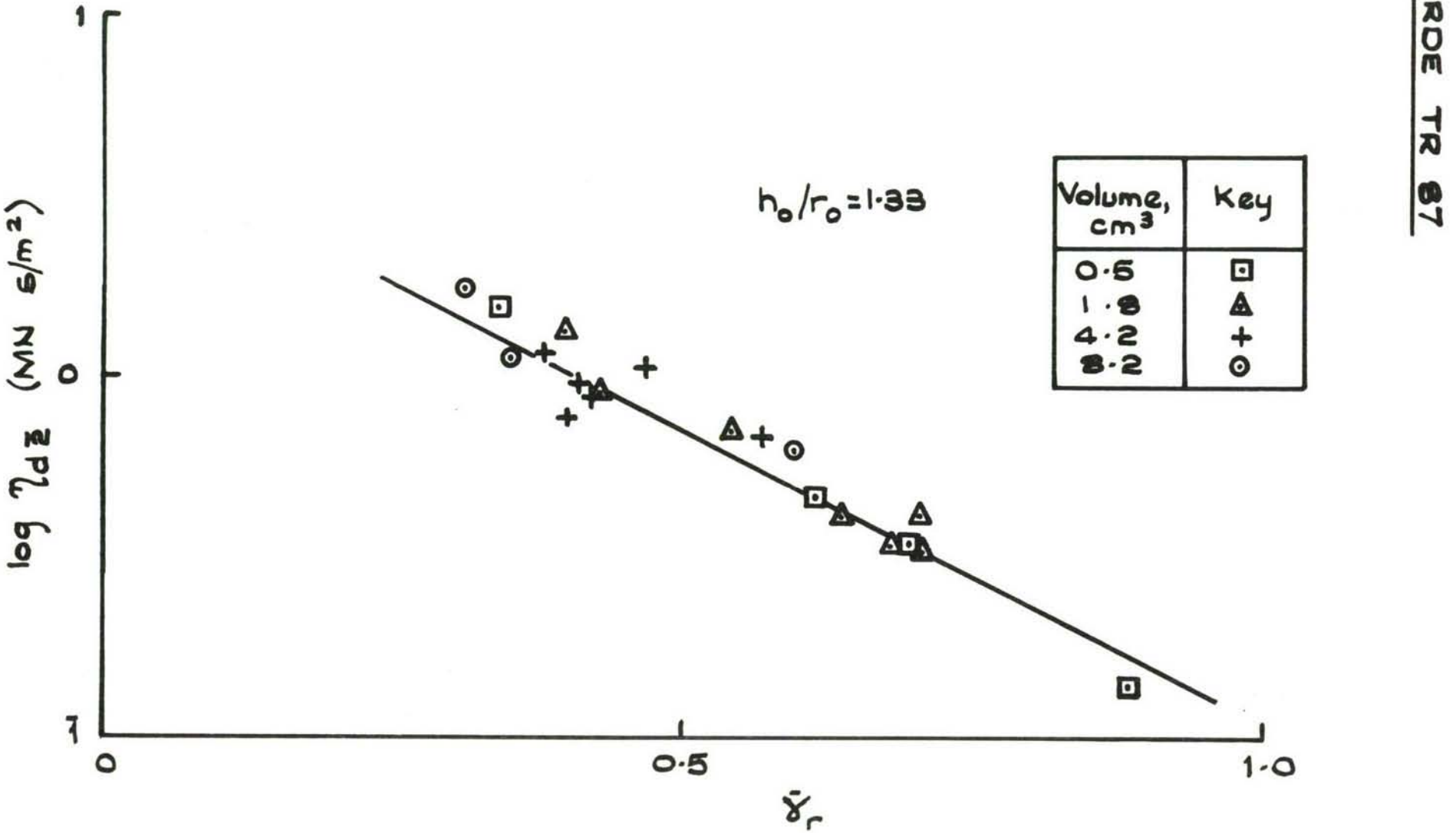

FIG. 10 THE EFFECT OF VOLUME AND MEAN STRAIN ON FINITE-STRAIN PLASTOVISCOSITY (STRAIN-RATE NORMALISED; INITIAL ASPECT RATIO CONSTANT)

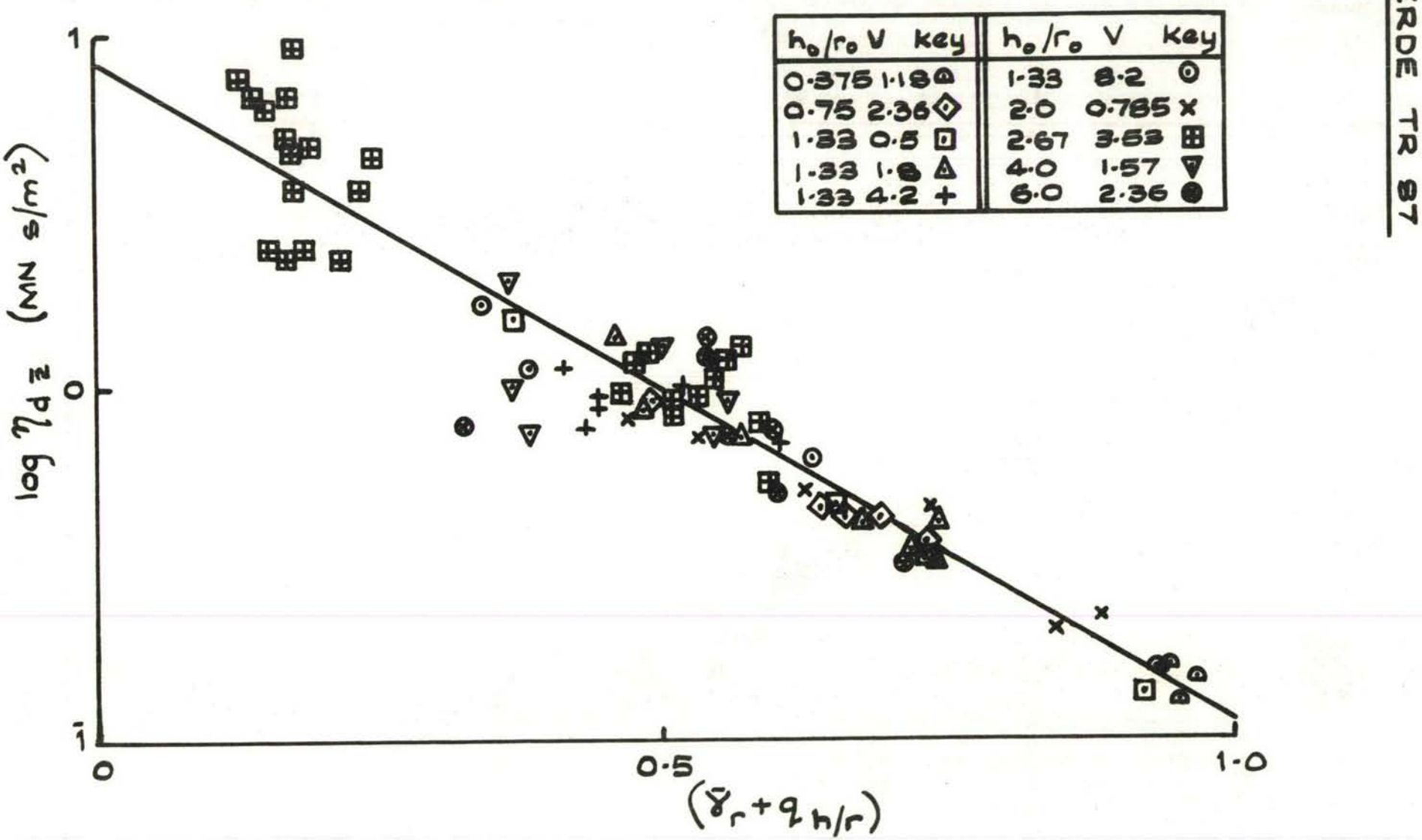

FIG. 11 THE EFFECT OF STRAIN (NORMALISED TO AN INITIAL ASPECT RATIO OF 1·55) ON FINITE-STRAIN PLASTOVISCOSITY (NORMALISED TO A STRAIN RATE OF 0·01 s^{-1})

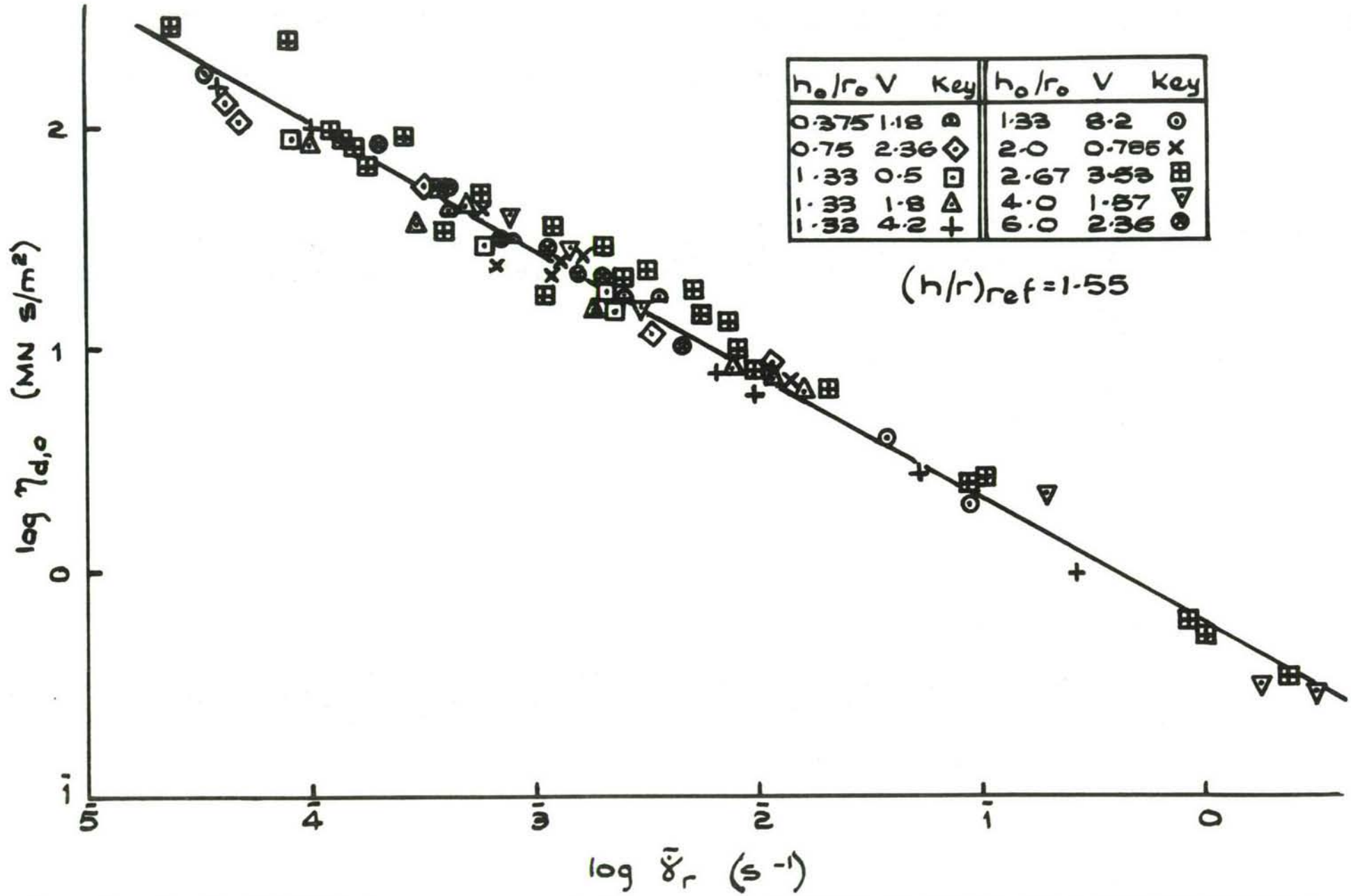

FIG. 12 THE EFFECT OF STRAIN-RATE ON FINITE-STRAIN PLASTOVISCOSITY (EXTRAPOLATED TO ZERO STRAIN AND NORMALISED TO AN INITIAL ASPECT RATIO OF 1·55)

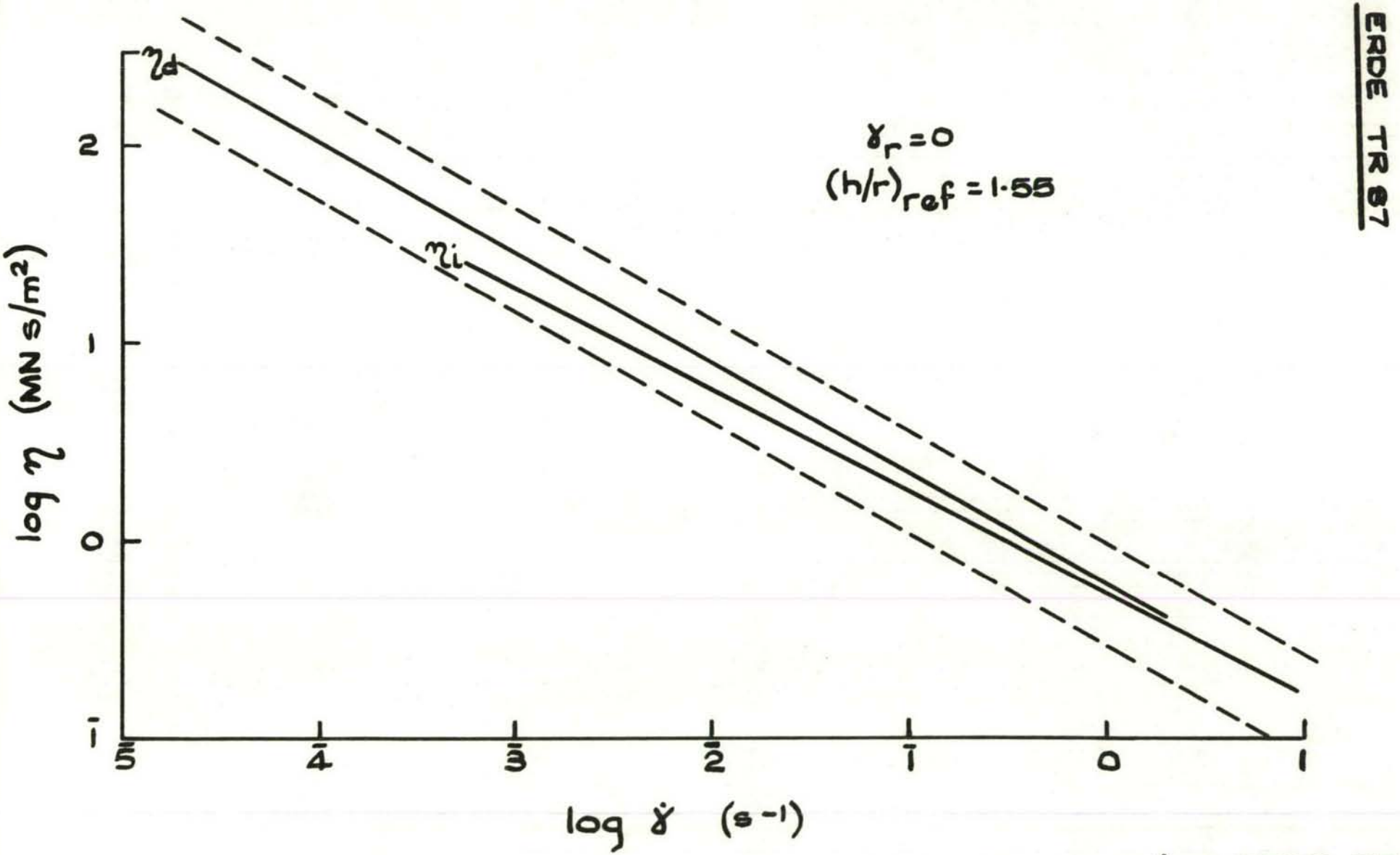

FIG.13 COMPARISON OF THE TWO EXPERIMENTAL METHODS (AT ZERO STRAIN AND NORMALISED TO AN INITIAL ASPECT RATIO OF 1·55)

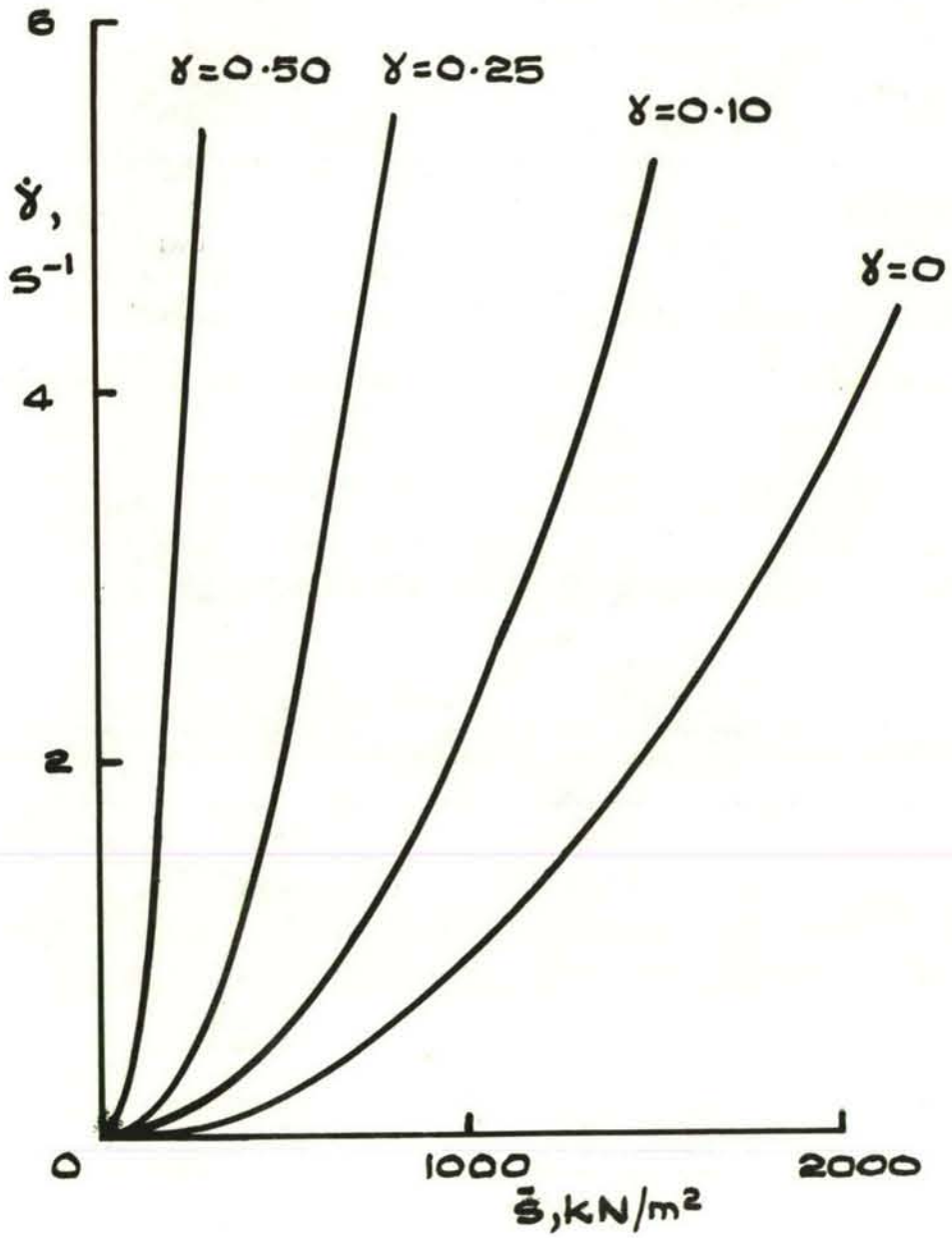

FIG. 14 THE FLOW CURVES OVER THE FULL EXPERIMENTAL STRAIN-RATE RANGE

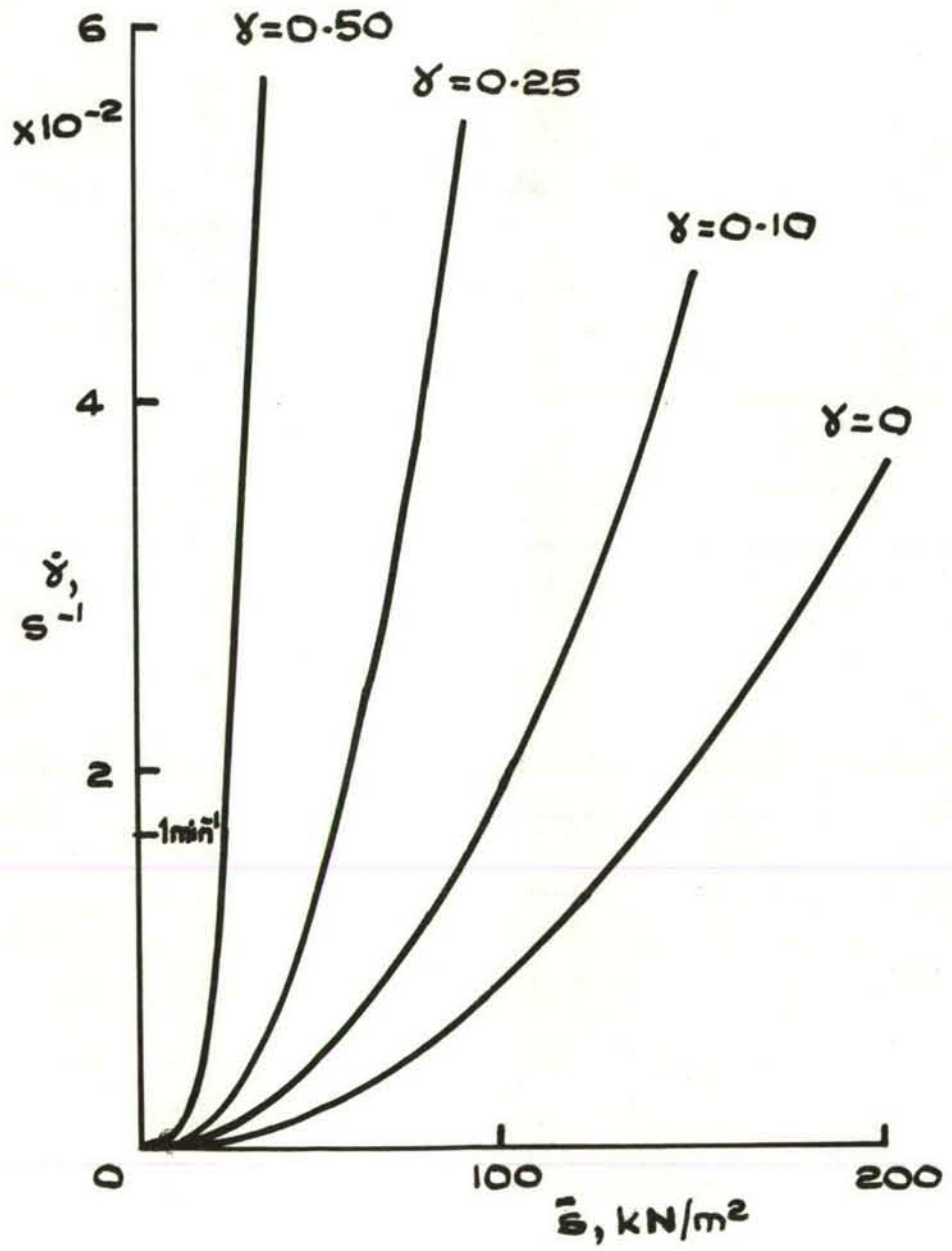

FIG. 15 ENLARGEMENT OF AREA NEAR THE ORIGIN OF FIG. 14

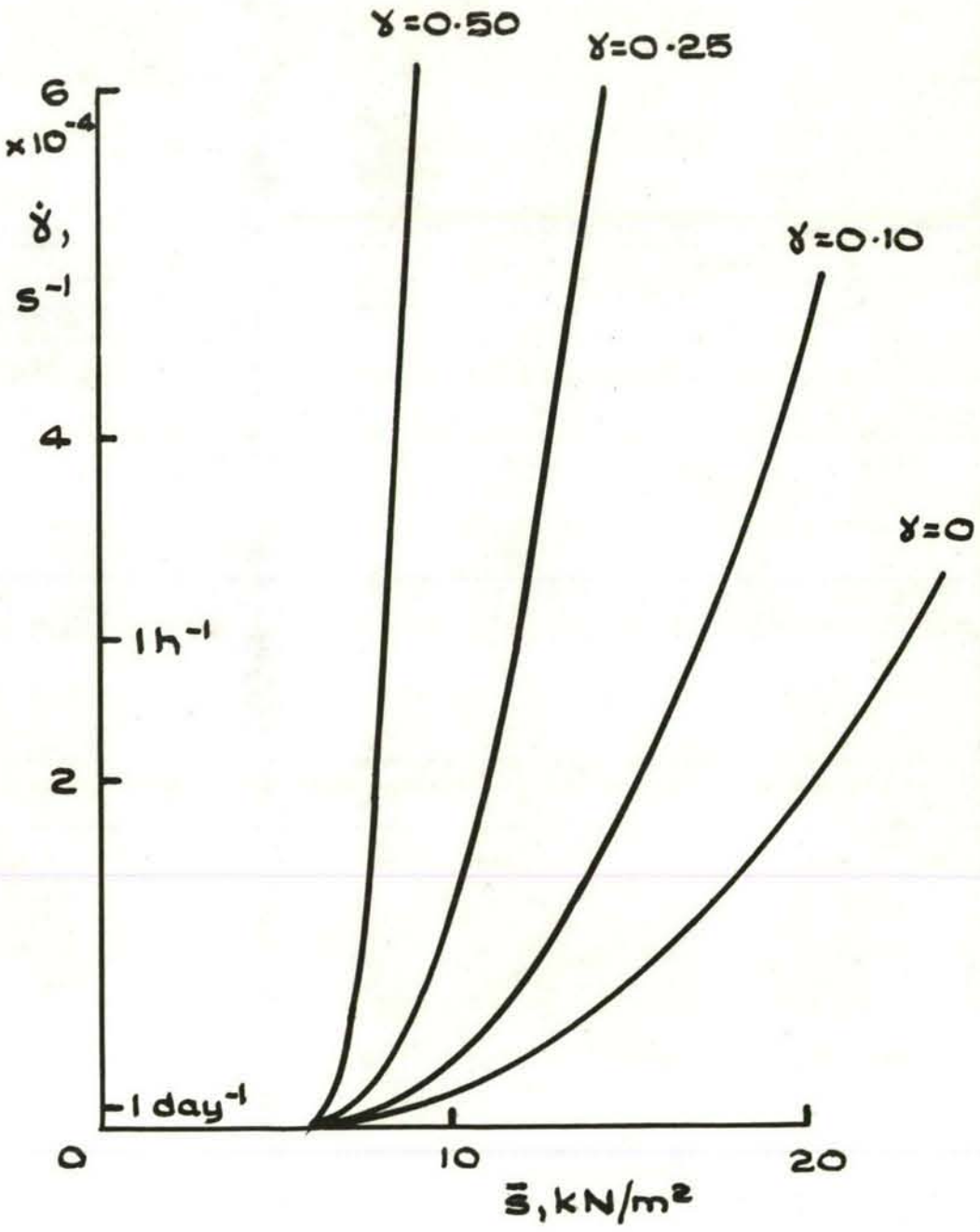

FIG. 16 ENLARGEMENT OF AREA NEAR THE ORIGIN OF FIG. 15

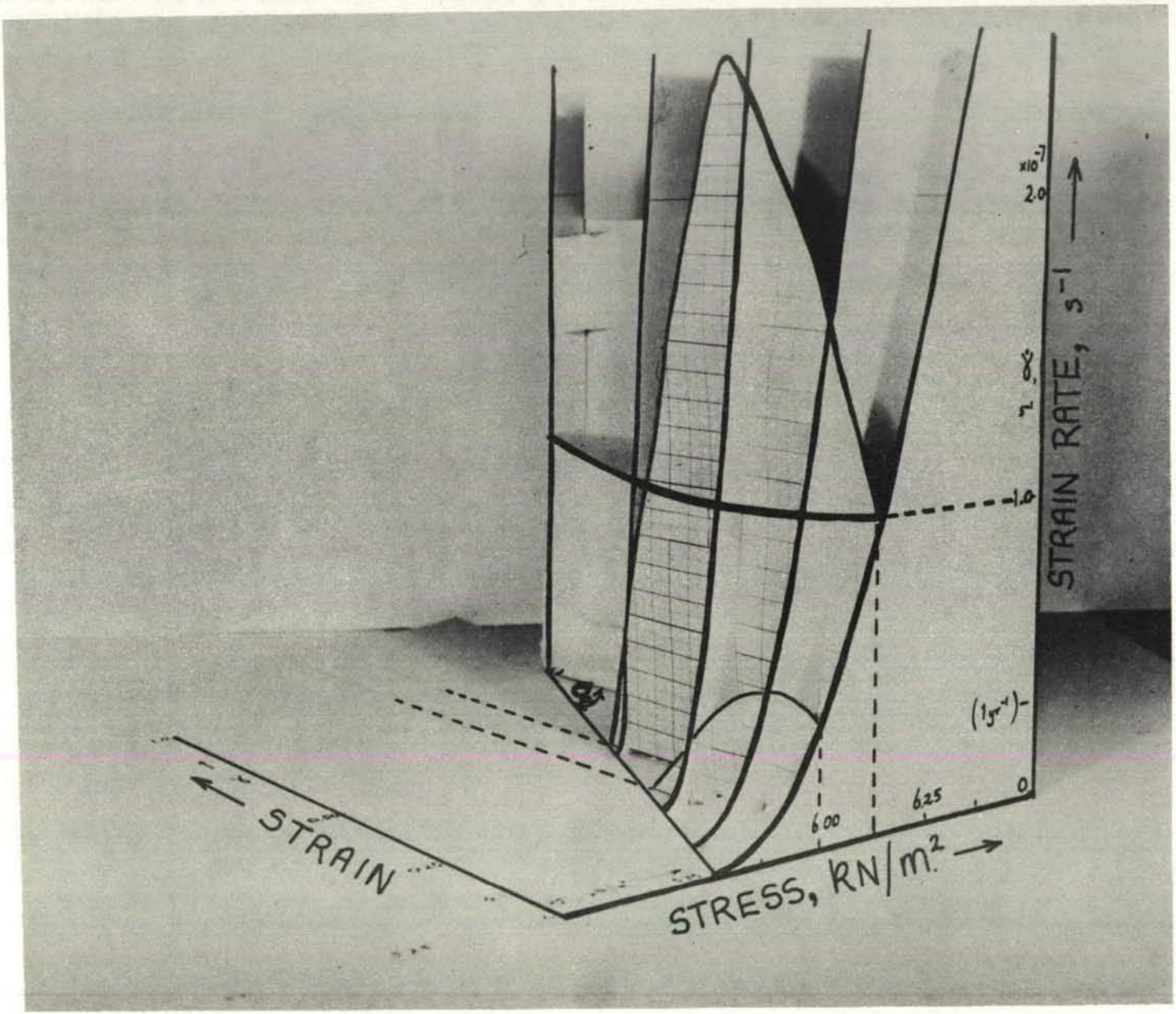

FIG. 17. MODEL OF FLOW CURVES EXTRAPOLATED TO VERY LOW STRESSES, APPROACHING THE YIELD STRESS.

Technical Report No 87
Explosives Research and Development Establishment
PARALLEL PLATE PLASTOMETRY OF PLASTIC PROPELLANT: PART 2:
DETERMINATION OF PLASTOVISCOSITY AND THE FLOW CURVE EQUATION
Gledhill Virginia M, Dukes W A
22 pp, no tabs, 17 figs

The use of the parallel-plate plastometer has been extended to measure the plastoviscosity of a representative plastic propellant over a wide strain-rate range (about 10^{-5} to 10 s^{-1}). The experimental technique is to compress a cylindrical specimen but the results can be analysed in two ways, yielding either zero-strain or finite-strain plastoviscosities respectively. Both plastoviscosities are, within experimental scatter, inversely proportional to the square root of the strain-rate, and range from about 100 to 0.1 MN s/m^2 (1 GP to 1 MP).

The plastoviscosity decreases rapidly and exponentially with increasing strain. When the finite-strain measurements are extrapolated to zero strain, there is good agreement with the zero-strain measurements.

/over

Technical Report No 87
Explosives Research and Development Establishment
PARALLEL PLATE PLASTOMETRY OF PLASTIC PROPELLANT: PART 2:
DETERMINATION OF PLASTOVISCOSITY AND THE FLOW CURVE EQUATION
Gledhill Virginia M, Dukes W A
22 pp, no tabs, 17 figs

The use of the parallel-plate plastometer has been extended to measure the plastoviscosity of a representative plastic propellant over a wide strain-rate range (about 10^{-5} to 10 s^{-1}). The experimental technique is to compress a cylindrical specimen but the results can be analysed in two ways, yielding either zero-strain or finite strain plastoviscosities respectively. Both plastoviscosities are, within experimental scatter, inversely proportional to the square root of the strain-rate, and range from about 100 to 0.1 MN s/m^2 (1 GP to 1 MP).

The plastoviscosity decreases rapidly and exponentially with increasing strain. When the finite-strain measurements are extrapolated to zero strain, there is good agreement with the zero-strain measurements.

/over

Technical Report No 87
Explosives Research and Development Establishment
PARALLEL PLATE PLASTOMETRY OF PLASTIC PROPELLANT: PART 2:
DETERMINATION OF PLASTOVISCOSITY AND THE FLOW CURVE EQUATION
Gledhill Virginia M, Dukes W A
22 pp, no tabs, 17 figs

The use of the parallel-plate plastometer has been extended to measure the plastoviscosity of a representative plastic propellant over a wide strain-rate range (about 10^{-5} to 10 s^{-1}). The experimental technique is to compress a cylindrical specimen but the results can be analysed in two ways, yielding either zero-strain or finite-strain plastoviscosities respectively. Both plastoviscosities are, within experimental scatter, inversely proportional to the square root of the strain-rate, and range from about 100 to 0.1 MN s/m^2 (1 GP to 1 MP).

The plastoviscosity decreases rapidly and exponentially with increasing strain. When the finite-strain measurements are extrapolated to zero strain, there is good agreement with the zero-strain measurements.

/over

Technical Report No 87
Explosives Research and Development Establishment
PARALLEL PLATE PLASTOMETRY OF PLASTIC PROPELLANT: PART 2:
DETERMINATION OF PLASTOVISCOSITY AND THE FLOW CURVE EQUATION
Gledhill Virginia M, Dukes W A
22 pp, no tabs, 17 figs

The use of the parallel plate plastometer has been extended to measure the plastoviscosity of a representative plastic propellant over a wide strain-rate range (about 10^{-5} to 10 s^{-1}). The experimental technique is to compress a cylindrical specimen but the results can be analysed in two ways, yielding either zero-strain or finite-strain plastoviscosities respectively. Both plastoviscosities are, within experimental scatter, inversely proportional to the square root of the strain-rate, and range from about 100 to 0.1 MN s/m^2 (1 GP to 1 MP).

The plastoviscosity decreases rapidly and exponentially with increasing strain. When the finite-strain measurements are extrapolated to zero strain, there is good agreement with the zero-strain measurements.

/over

The flow curve for a given strain, relating strain-rate with stress, is parabolic. The yield stress and shear-hardening coefficient (measured separately) have been taken into account, resulting in a complete flow equation linking stress, strain and strain-rate, corresponding to a family of flow curves.

The flow curve for a given strain, relating strain-rate with stress, is parabolic. The yield stress and shear-hardening coefficient (measured separately) have been taken into account, resulting in a complete flow equation linking stress, strain and strain-rate, corresponding to a family of flow curves.

The flow curve for a given strain, relating strain-rate with stress, is parabolic. The yield stress and shear-hardening coefficient (measured separately) have been taken into account, resulting in a complete flow equation linking stress, strain and strain-rate, corresponding to a family of flow curves.

The flow curve for a given strain, relating strain-rate with stress, is parabolic. The yield stress and shear-hardening coefficient (measured separately) have been taken into account, resulting in a complete flow equation linking stress, strain and strain-rate, corresponding to a family of flow curves.